THE PLANT CELL

Research Article

The Arabidopsis MATERNAL EFFECT EMBRYO ARREST45 protein modulates maternal auxin biosynthesis and controls seed size by inducing AINTEGUMENTA

Ying Ju Li [1,**] Yang Yu [1,**] Xiuying Liu [2] Xian Sheng Zhang [1,*] and Ying Hua Su [1,*,‡]

1   State Key Laboratory of Crop Biology, College of Life Sciences, Shandong Agricultural University, Tai'an, 271018, Shandong, China
2   Novogene Bioinformatics Institute, Beijing, 100020, China

*Authors for Correspondence: suyh@sdau.edu.cn; zhangxs@sdau.edu.cn
**These authors contributed equally to this work.
†Senior author.
Y.H.S. and X.S.Z. designed the research and wrote the manuscript. Y.J.L. and Y.Y. performed the experiments. X.L. analyzed the RNA-seq data.
The author responsible for the distribution of materials integral to the findings presented in this article in accordance with the policy described in the Instructions for Authors (https://academic.oup.com/plcell) is: Ying Hua Su (suyh@sdau.edu.cn).

Abstract

Seed size is a major factor determining crop yields that is controlled through the coordinated development of maternal and zygotic tissues. Here, we identified Arabidopsis MATERNAL EFFECT EMBRYO ARREST45 (MEE45) as a B3 transcription factor that controls cell proliferation and maternally regulates seed size through its transcriptional activation of AINTEGUMENTA (ANT) and its downstream control of auxin biosynthesis in the ovule integument. After characterizing reduced seed and organ size phenotypes in mee45 mutants and finding that overexpression of MEE45 causes oversized seeds, we discovered that the MEE45 protein can bind to the promoter region of the ANT locus and positively regulate its transcription. ANT in-turn activates the expression of auxin biosynthetic genes (e.g. YUCCA4) in the ovule integument. Our results thus illustrate mechanisms underlying maternal tissue-mediated regulation of seed size and suggest that MEE45 and its downstream components can be harnessed to develop higher-yielding crop varieties.

Introduction

Seed size is a vital agronomic trait and determinant of crop yield (Moles et al., 2005; Adamski et al., 2009; Li and Li, 2016). Increasing seed size would provide an efficient method to raise grain yield and to meet the dietary caloric demands of the growing population worldwide (Khush, 2003; Song et al., 2007; Shomura et al., 2008; Fan et al., 2009; Zuo and Li, 2014). Accordingly, the regulation of seed size has been extensively studied in plant and crop sciences.

Seed size is determined by the coordinated development of maternal and zygotic tissues. In angiosperms, the zygotic tissues result from double fertilization, when one male sperm cell fuses with the two female polar nuclei to produce the triploid endosperm, while the other sperm cell combines with the egg to form the diploid embryo (Chaudhury et al., 2001; He et al., 2017). The seed coat is the maternal sporophytic tissue of the seed: it surrounds the embryo and endosperm, and is derived from the integument of the ovule (Haughn and Chaudhury, 2005). The integument forms the cavity within which the embryo and the

Open Access

IN A NUTSHELL

Background: Seed size is determined by the coordinated development of maternal and zygotic tissues. The diploid embryo, the triploid endosperm, and the maternal ovule integument coordinate their development to determine the final size of the seed. In Arabidopsis (*Arabidopsis thaliana*), a number of factors act through maternal tissues (ovule) to control seed size. The *AINTEGUMENTA* (*ANT*) gene encodes an AP2-domain transcription factor that acts maternally to control seed size. *maternal effect embryo arrest* (*mee*) mutants have been identified based on their phenotypes during embryogenesis that are caused by effects on maternal tissues. Although many genes regulate seed size through maternal tissues in Arabidopsis, it is still unclear how seed size is maternally controlled, and how ovules and embryos coordinate their growth to determine final seed size.

Question: We wanted to know how genes participate in the maternal control of seed size. We searched for mutants with small-sized seed phenotypes in the collection of *mee* mutants, and studied the function of one candidate by characterization of the mutant and overexpression lines.

Findings: We identified the B3-type transcription factor MEE45 as a seed size regulator. MEE45 controls cell proliferation in the ovule integument and affects final seed size. Moreover, MEE45 directly binds to the promoter region of *ANT* to activate its transcription. We also showed that auxin biosynthesis capacity in ovules—as represented by the expression of the auxin biosynthesis gene *YUCCA4* and free auxin levels—is regulated by a MEE45-*ANT* pathway. These results support maternally-controlled embryo development and seed size determination. Our study provides a deeper understanding of maternal tissue-mediated regulation of seed size and suggests that MEE45 manipulation may be a useful tool for the improvement of crop seed production.

Next steps: Understanding the genetic and molecular basis of seed size control will help scientists utilize beneficial seed size genes to improve crop yield. Next, we wish to manipulate MEE45 and/or related pathways and components in crops, which may enable new technologies to increase seed yields in crop production.

endosperm will grow after fertilization, and become the seed coat that sets a physical constraint on final seed size (Adamski et al., 2009; Fang et al., 2012; Xia et al., 2013; Du et al., 2014). The diploid embryo, the triploid endosperm, and the maternal integument coordinate their development to determine the final size of the seed.

In Arabidopsis (*Arabidopsis thaliana*), several factors act through maternal tissues to control seed size (Jofuku et al., 2005; Ohto et al., 2005; Li et al., 2008; Adamski et al., 2009; Xia et al., 2013). The WRKY family transcription factor TRANSPARENT TESTA GLABRA2 promotes cell expansion in the ovule integument for seed growth (Garcia et al., 2005; Ohto et al., 2009). In contrast, the ubiquitin receptor DA1 (meaning large in Chinese) restricts cell proliferation in the integument of the developing ovule to physically limit seed size through the seed coat after fertilization (Li et al., 2008; Xia et al., 2013). The APETALA 2 (AP2) transcription factor controls seed size by limiting cell expansion in the ovule integument (Jofuku et al., 2005; Ohto et al., 2005, 2009). The *AINTEGUMENTA* (*ANT*) gene encodes an AP2-domain transcription factor (Weigel, 1995; Elliott et al., 1996; Klucher et al., 1996). Like the *da1* and *ap2* mutants, plants overexpressing *ANT* produce oversized organs and seeds (Mizukami and Fischer, 2000). Since ANT is a regulator of ovule integument initiation and ovule development (Elliott et al., 1996; Klucher et al., 1996), it acts maternally to control seed size (Li and Li, 2015).

The plant phytohormone auxin also regulates seed development. Among the 23 Arabidopsis *AUXIN RESPONSE FACTOR* (*ARF*) genes, which function in auxin-mediated gene expression, *ARF2* is known to control seed size by restricting cell proliferation of the ovule integument (Schruff et al., 2006). Plants carrying mutations in the gene encoding the receptor kinase FERONIA (FER), which mediates auxin-regulated root hair growth (Duan et al., 2010; Westermann et al., 2019), produce seeds of larger size relative to the wild-type (WT) by increasing cell expansion in the ovule integuments (Yu et al., 2014). In rice (*Oryza sativa*), overexpression of *BIG GRAIN1*, which encodes a factor that participates in auxin transport, significantly increases grain size by promoting cell proliferation and expansion in spikelet hulls (Liu et al., 2015b) Thus, auxin signaling and transport appear to set a physical restriction for seed growth and seed size via the seed coat. A recent study showed that the ovule integuments affect seed development by supplying maternally produced auxin to the early embryo, suggesting that auxin from maternal tissues is apparently required for normal embryo development (Robert et al., 2018).

Loss-of-function mutations in the *MATERNAL EFFECT EMBRYO ARREST* (*MEE*) loci, identified based on defects in female gametophyte development by a Dissociation (DS) transposon insertion screen, exhibit defects in embryogenesis (Pagnussat et al., 2005). Here, we show that MEE45, a B3-type transcription factor, is required for ovule integument initiation and development. MEE45 is a seed size regulator that controls cell proliferation in the maternal integument and affects final seed size. Moreover, we determined that MEE45 directly binds to the promoter region of the *ANT* locus to activate *ANT* transcription. We also showed that the auxin biosynthesis capacity of maternal cells—as represented
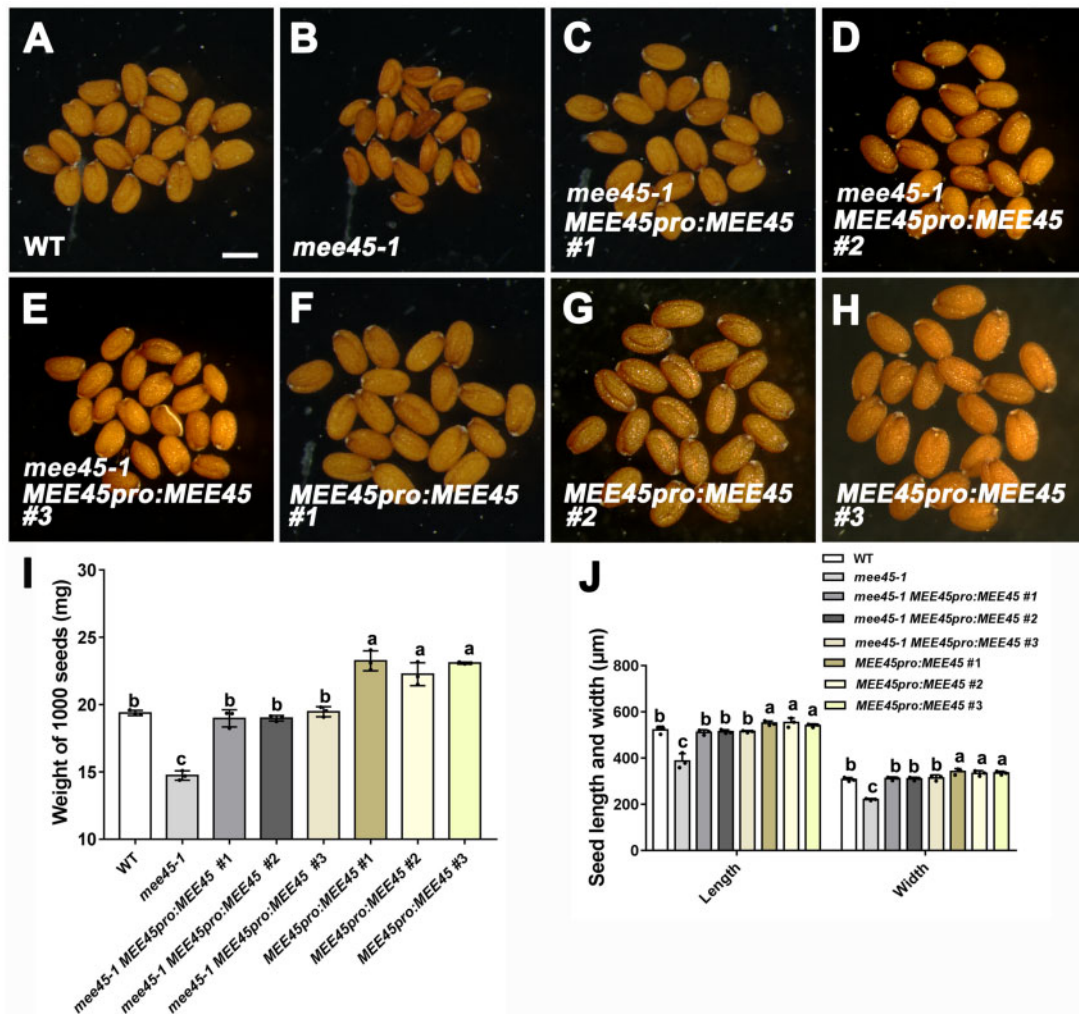
Figure 1 MEE45 regulates seed size. A–H, Mature dry seeds of the WT (Col-0) (A), *mee45-1* (B), *mee45-1 MEE45pro:MEE45* line #1 (C), *mee45-1 MEE45pro:MEE45* line #2 (D), *mee45-1 MEE45pro:MEE45* #3 (E), *MEE45pro:MEE45* line #1 (F), *MEE45pro:MEE45* line #2 (G) and *MEE45pro:MEE45* line #3 (H), Bar = 500 μm. I, Average seed mass per 1,000 seeds of the WT, *mee45-1*, *mee45-1 MEE45pro:MEE45* and *MEE45pro:MEE45* lines. J, Average seed length and width of the WT, *mee45-1*, *mee45-1 MEE45pro:MEE45*, and *MEE45pro:MEE45* lines. The error bars in (I) and (J) represent the standard error of the mean, which were calculated from three sets of biological replicates. One-way analysis of variance (ANOVA) and Tukey's multiple comparison tests were performed. Statistically significant differences are indicated by different lowercase letters ($P < 0.05$).

by the expression levels of the auxin biosynthetic gene *YUCCA4* (*YUC4*)—is regulated by a MEE45–ANT regulatory module to support maternally controlled embryo development and seed size determination.

Results

MEE45 functions in controlling seed size

To genetically dissect the mechanisms of maternally controlled seed size, we collected Arabidopsis T-DNA insertion lines in predicted *MEE* genes with documented expression in ovules and/or embryos across several microarray studies. Phenotypic analysis of this collection of lines allowed the identification of three T-DNA insertion mutants in *MEE45* (*mee45-1*, SALK_031530; *mee45-2*, SALK_038324; *mee45-3*, CS801014) with obvious seed growth defects. *MEE45* encodes a B3-type transcription factor of unknown biological function (Supplemental Figure S1A). *MEE45* transcript levels

in mature ovules of *mee45-1* mutant plants were significantly reduced compared to levels in the WT Columbia-0 (Col-0) (Supplemental Figure S1B). Seeds of the *mee45-1* mutant were significantly smaller and lighter than those from the WT (Figure 1, A, B, I, and J; Supplemental Data Sets S1 and S2), but showed no significant difference in their seed germination rate or viability compared to the WT (Supplemental Figure S2, A, B, D, E, G, and H; Supplemental Data Sets S3 and S4). The embryo occupies the majority of the mature seed in Arabidopsis. To identify the cellular basis of the small seed phenotype of the *mee45-1* mutant, we compared embryo sizes between *mee45-1* and the WT. The *mee45-1* mutant produced significantly smaller embryos relative to those of the WT, from the early globular embryo stage up to the mature embryo stage (Figure 2). However, embryo morphology was broadly comparable between the mutant and the WT at each developmental stage.
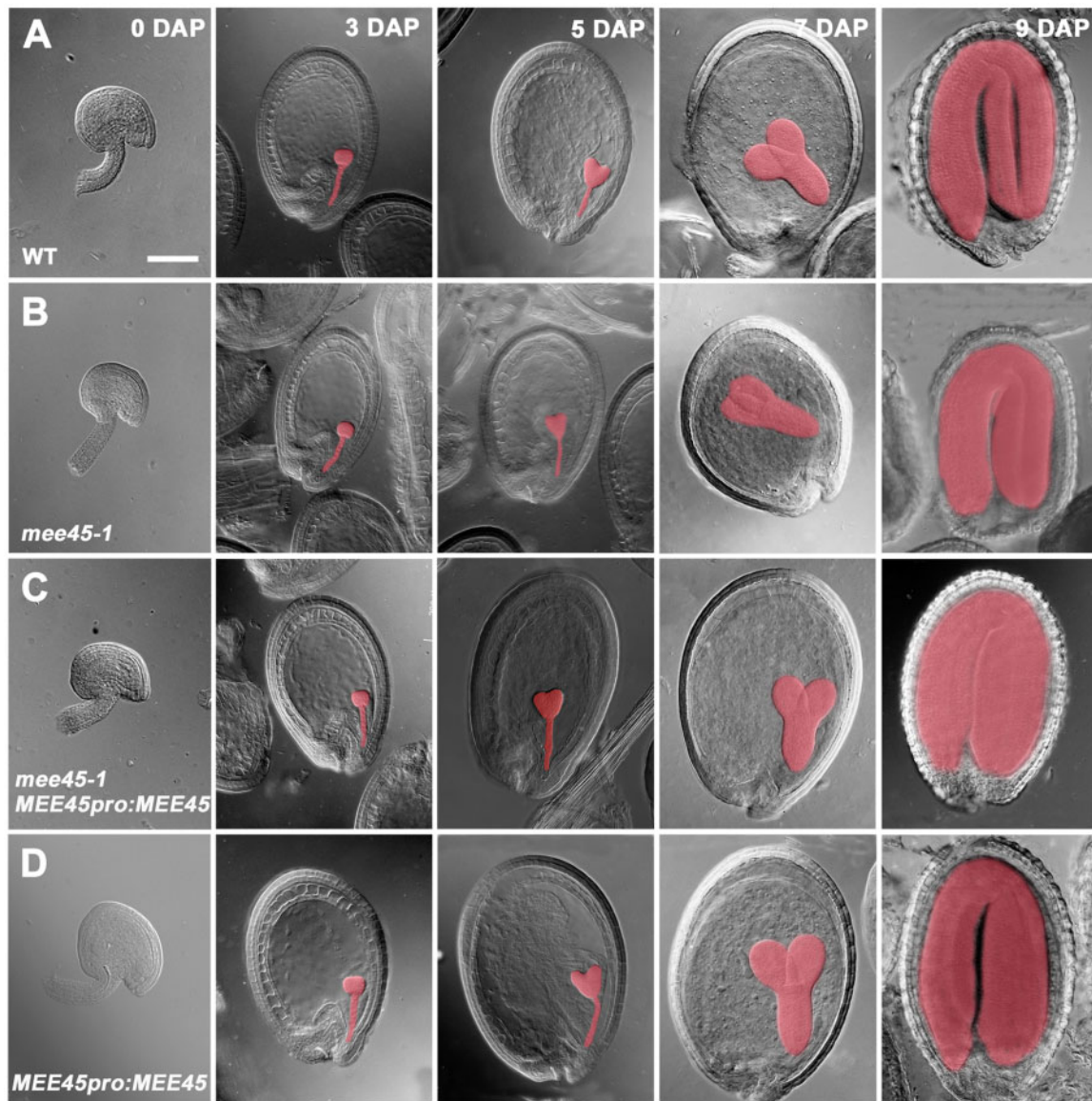
Figure 2 Embryo development in WT, *mee45-1*, *mee45-1 MEE45pro:MEE45* and *MEE45pro:MEE45* plants. Whole-mount seeds observed by DIC microscopy at 0, 3, 5, 7, and 9 days after pollination (DAP) in the WT (A), *mee45-1* (B), *mee45-1 MEE45pro:MEE45* (C), and *MEE45pro:MEE45* plants (D). Bar = 100 µm.

In contrast to the *mee45-1* mutant, both *mee45-2* and *mee45-3* mutants accumulated extremely low levels of *MEE45* transcripts, and were thus assumed to be knockout mutants (Supplemental Figure S1, A and B). Approximately 70%–80% mutant seeds of *mee45-2* or *mee45-3* were significantly smaller than those of the WT (Supplemental Figure S1, C–I; Supplemental Data Sets S5 and S6), although ~75%–85% embryos in each mutant showed normal developmental patterns (Supplemental Figure S3, B and D). However, roughly 12%–20% embryos from each mutant displayed clear developmental defects as early as the globular stage (Supplemental Figure S3, C and E). Because of these additional developmental phenotypes affecting embryo morphology, we focused our subsequent investigations on the *mee45-1* mutant for further analysis of seed size regulation.

The small seed phenotype observed in *mee45-1* was rescued by the transgenic expression of *MEE45* under the control of its own promoter (*mee45-1 MEE45pro:MEE45*; Figure 1, C–E, I, and J; Supplemental Figure S4; Supplemental Data Sets S1 and S2), confirming the role of MEE45 in the control of seed size. Moreover, we also found that transgenic lines with *MEE45pro:MEE45* in the WT background produced seeds that were significantly larger and heavier relative to Col-0 seeds (Figure 1, F–J; Supplemental Figure S4; Supplemental Data Sets S1 and S2), and with oversized embryos from the early globular embryo stage up to the mature embryo stage (Figure 2). These results confirm that MEE45 exerts a function in mediating seed size and seed mass.

We measured the size and number of cotyledon epidermal cells of mature embryos in *mee45-1* and the WT: we

observed an increase in cell size that was accompanied by a significant decrease in cell number in the cotyledons of *mee45-1* embryos as compared to the WT (Supplemental Figure S5; Supplemental Data Sets S7–S9). These findings suggest that a reduction in cell proliferation in embryos is responsible for the small seed size of *mee45-1* plants.

Although the embryo was smaller in the mutant background, the endosperm in *mee45-1* did not appear substantially different from that of the WT (Supplemental Figure S6, A–F). Moreover, there was no difference between *mee45-1* mutant and WT seeds for the expression levels of genes known to mediate endosperm development (e.g. *MINISEED3* [*MINI3*], *HAIKU1* and *2* [*IKU1/2*], and *SHORT HYPOCOTYL UNDER BLUE1* [*SHB1*]) (Zhou et al., 2009; Kang et al., 2013) (Supplemental Figure S6G).

To examine the effects of MEE45 function on organ growth in more detail, we measured the expression of *MEE45* and found it to be much higher in leaves, flowers,

and siliques than in roots (Supplemental Figure S7). We then evaluated the size of these organs in the *mee45-1* mutant. Leaves, floral organs, and siliques were significantly smaller in the *mee45-1* mutant compared to WT plants, without obvious alterations of their overall morphology at different developmental stages (Supplemental Figure S8; Supplemental Data Sets S10 and S11). These results support the notion that MEE45 contributes to the regulation of organ size in Arabidopsis.

MEE45 acts maternally to influence seed size

To determine whether the small seed phenotype of the *mee45* mutant originated from maternal (the ovule) or zygotic tissues (the embryo), we performed reciprocal crossing experiments between *mee45* and the WT Col-0. As shown in Figure 3 and Table 1, we only noticed the effects of the *mee45* mutation on seed size when maternal plants were
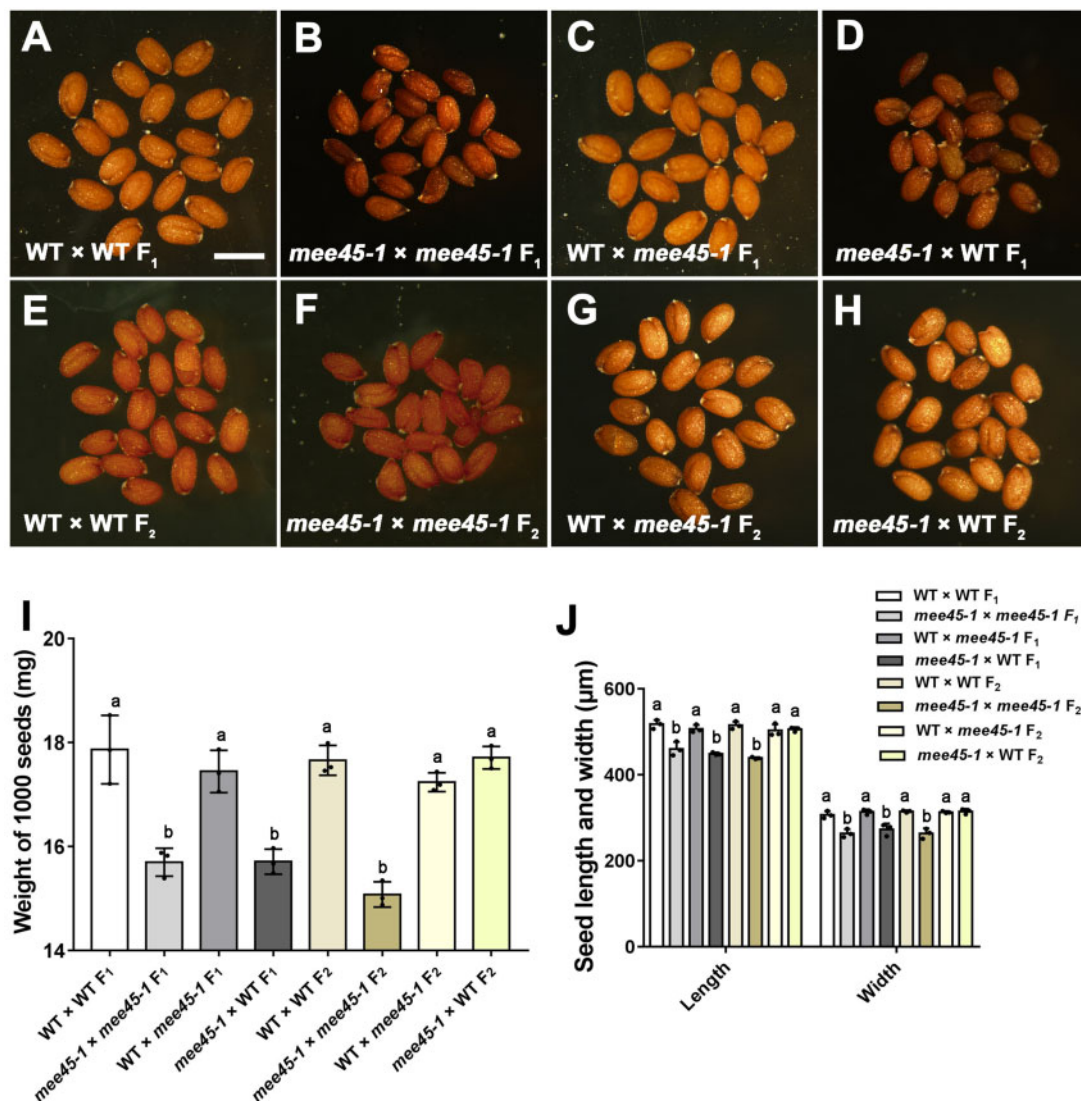
Figure 3 MEE45 maternally controls seed size. A–H, Mature dry seeds of [WT × WT] F_1 (A), [*mee45-1* × *mee45-1*] F_1 (B), [WT × *mee45-1*] F_1 (C), [*mee45-1* × WT] F_1 (D), [WT × WT] F_2 (E), [*mee45-1* × *mee45-1*] F_2 (F), [WT × *mee45-1*] F_2 (G) and [*mee45-1* × WT] F_2 (H) plants. Bar = 500 μm. I, Average seed mass per 1,000 seeds of the indicated genotypes. J, Average seed length and width of the indicated genotypes. The error bars in (I) and (J) represent the standard error of the mean, calculated from three sets of biological replicates. One-way ANOVA and Tukey's multiple comparison tests were performed. Statistically significant differences are indicated by different lowercase letters ($P < 0.05$).

Table 1 Maternal effects of MEE45 in controlling seed size

| Cross Group♀× ♂	Cross Number	Zygote	Maternal Sporophyte	Seed Phenotype
Col-0 × mee45-1−/− F₁	1	+/−	+/+	Normal, $n = 51$
	2	+/−	+/+	Normal, $n = 48$
	3	+/−	+/+	Normal, $n = 55$
mee45-1⁻/⁻ × Col-0 F₁	4	+/−	−/−	Small, $n = 55$
	5	+/−	−/−	Small, $n = 54$
	6	+/−	−/−	Small, $n = 53$
Col-0 × mee45-1⁻/⁻ F₂	7	+/+	+/−	Normal, $n = 12$
		+/−	+/−	Normal, $n = 25$
		−/−	+/−	Normal, $n = 11$
	8	+/+	+/−	Normal, $n = 13$
		+/−	+/−	Normal, $n = 24$
		−/−	+/−	Normal, $n = 12$
	9	+/+	+/−	Normal, $n = 13$
		+/−	+/−	Normal, $n = 23$
		−/−	+/−	Normal, $n = 12$
mee45-1⁻/⁻ × Col-0 F₂	10	+/+	+/−	Normal, $n = 10$
		+/−	+/−	Normal, $n = 22$
		−/−	+/−	Normal, $n = 12$
	11	+/+	+/−	Normal, $n = 12$
		+/−	+/−	Normal, $n = 21$
		−/−	+/−	Normal, $n = 14$
	12	+/+	+/−	Normal, $n = 11$
		+/−	+/−	Normal, $n = 24$
		−/−	+/−	Normal, $n = 14$

homozygous for the *mee45-1* mutation. Seeds produced by homozygous *mee45-1* maternal plants were consistently smaller than those produced by WT maternal plants, regardless of the genotype of the pollen donor (Figure 3, A–D, I, and J; Supplemental Data Sets S12 and S13). Furthermore, heterozygous F₁ seeds derived from either a cross between a WT maternal parent and a *mee45-1* pollen donor or between a *mee45-1* maternal parent and a WT pollen donor produced F₂ seeds with normal seed size, even for the 25% of the seeds that were homozygous for the *mee45-1* mutation (Figure 3, E–J; Table 1; Supplemental Data Sets S12 and S13). Additionally, we observed the small seed phenotype and defects in seed development in heterozygous F₁ seeds only when maternal plants were homozygous for the *mee45-2* or *mee45-3* mutations (Supplemental Figures S9 and S10; Supplemental Data Sets S14–S17). These results clearly indicate that the maternal genotype at the *MEE45* locus determines the seed size in the next generation.

To investigate the accumulation patterns of the MEE45 protein, we introduced a transgene in WT plants consisting of the *MEE45* coding sequence (CDS) cloned in frame with the green fluorescent protein (*GFP*) gene and placed under the control of the *MEE45* promoter. We then detected the GFP signal in these *gMEE45-GFP* transgenic plants. As expected for a transcription factor, MEE45-GFP accumulated in the nucleus. The MEE45-GFP signal was strong during ovule development (Figure 4, A–D). We detected GFP fluorescence throughout the entire ovule primordium, as well as in the megasporocyte, the nucellus, and at the base of the nucellus where the inner and outer integument initiate (Figure 4, A and B). During the mature stages (3-IV and 3-VI) of ovule development, MEE45-GFP accumulated in the

embryo sac, ovule integument, and the funiculus (Figure 4, C and D). After fertilization, we observed MEE45-GFP fluorescence in the seed coat, as well as in the embryo (Figure 4E).

To investigate whether *MEE45* expression in the integument of the ovule might be responsible for regulating seed size, we specifically expressed *MEE45* in the integument of the *mee45-1* mutant by using the *INNER NO OUTER* (*INO*) promoter (Supplemental Figure S11, A–C), which is strictly expressed in the ovule integument (Meister et al., 2002; Wang et al., 2016). *INOpro:MEE45* expression completely rescued the small seed phenotype seen in the *mee45-1* mutant, and resulted in normal seed sizes comparable to those of the WT (Figure 4, F–H, K, and L; Supplemental Data Set S19). Note that these findings are similar to the results obtained when *MEE45* was driven by its own promoter (Figure 1, A–E). Moreover, *INOpro:MEE45* transgenic lines in the WT background produced significantly oversized seeds (Figure 4, F, I, K, and L; Supplemental Data Set S19).

We also specifically reduced *MEE45* transcript levels in seeds by using the *RIBOSOMAL PROTEIN S5A* (*RPS5A*) promoter (Supplemental Figure S11D), which is strictly expressed in the embryos and endosperm of seeds after fertilization (Weijers et al., 2001; Zhang et al., 2017), to drive the expression of an artificial microRNA (amiRNA) targeting *MEE45*. *RPS5Apro:amiRNA-MEE45* transgenic lines produced normal-sized seeds showing no significant difference with those of the WT (Figure 4, F, J, K, and L; Supplemental Data Set S19), suggesting that the expression of *MEE45* in the embryo does not contribute to its function in regulating seed size. Together, these results indicate that *MEE45* functions in ovule integuments for the maternal control of seed size.
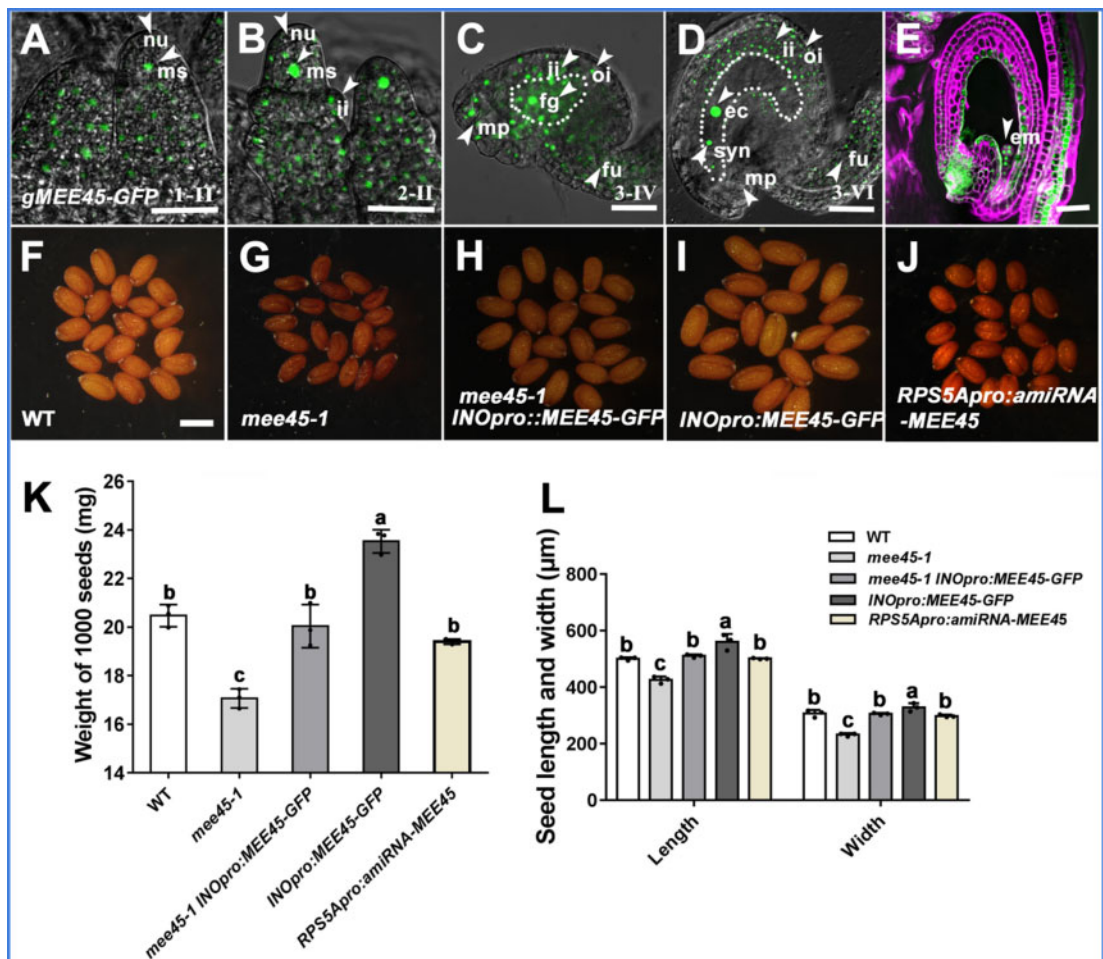
Figure 4 MEE45 functions in the ovule integument for the maternal control of seed size. A–E, Accumulation pattern of MEE45 in developing ovules (1-II (A), 2-II (B), 3-IV (C), and 3-VI (D) mature ovule stages) and seeds (2 DAP) (E) of *gMEE45-GFP* transgenic plants. Bars = 100 μm. nu, nucellus; ms, megasporocyte; ii, inner integument; oi, outer integument; fg, female gametophyte; ec, egg cell; syn, synergid; mp, micropyle; fu, funiculus; em, embryo . F–J, Mature dry seeds of the WT (F), *mee45-1* (G), *mee45-1 INOpro:MEE45-GFP* (H), *INOpro:MEE45-GFP* (I), and *RPS5Apro:amiRNA-MEE45* (J) plants. Bar = 750 μm. K, Average seed mass per 1,000 seeds of the indicated genotypes. L, Average seed length and width of the indicated genotypes. The error bars in (K) and (L) represent the standard error of the mean, calculated from three sets of biological replicates. One-way ANOVA and Tukey's multiple comparison tests were performed. Statistically significant differences are indicated by different lowercase letters ($P < 0.05$).

MEE45 induces cell proliferation in the ovule integument

The ovule is a precursor of the seed and its maternal tissues affect both seed development and size (Xia et al., 2013; Du et al., 2014). Thus, we examined ovule size and discovered that it was significantly smaller in the *mee45-1* mutant than in the WT (Figure 5, A and B). We also observed that the number of cells in the outer integument layer of mutant ovules was significantly lower compared to WT ovules. Consequently, the length of the outer integument in the mutant was much shorter than in the WT (Figure 5, C and D; Supplemental Data Sets S20 and S21). The *CYCLIN B1;1* (*CYCB1;1*) gene is expressed at the G2/M phase of the cell cycle, and its expression has provided a useful marker to study cell proliferation during organ development (Schnittger and De Veylder, 2018). We compared the staining pattern of the *CYCB1;1pro:β-GLUCURONIDASE* (*GUS*) reporter in the ovules of *mee45-1* and WT plants (Supplemental Figure S12). In mature ovules of the WT, there was strong GUS staining in the nucellus and in the integument cells enclosing it (Supplemental Figure S12A). In contrast, we detected hardly any GUS staining in ovule integument cells of the *mee45-1* mutant, and these plants had only very weak GUS staining in the nucellus (Supplemental Figure S12B). Thus, our results demonstrate that MEE45 induces cell proliferation in the ovule, especially in the integument.

Next, we compared ovule developmental progression between the *mee45-1* mutant and the WT. The initiation and development of both the inner and the outer integuments in the *mee45-1* mutant were significantly delayed relative to the WT (Figure 5, E–H). In stage 10 carpels of both WT and
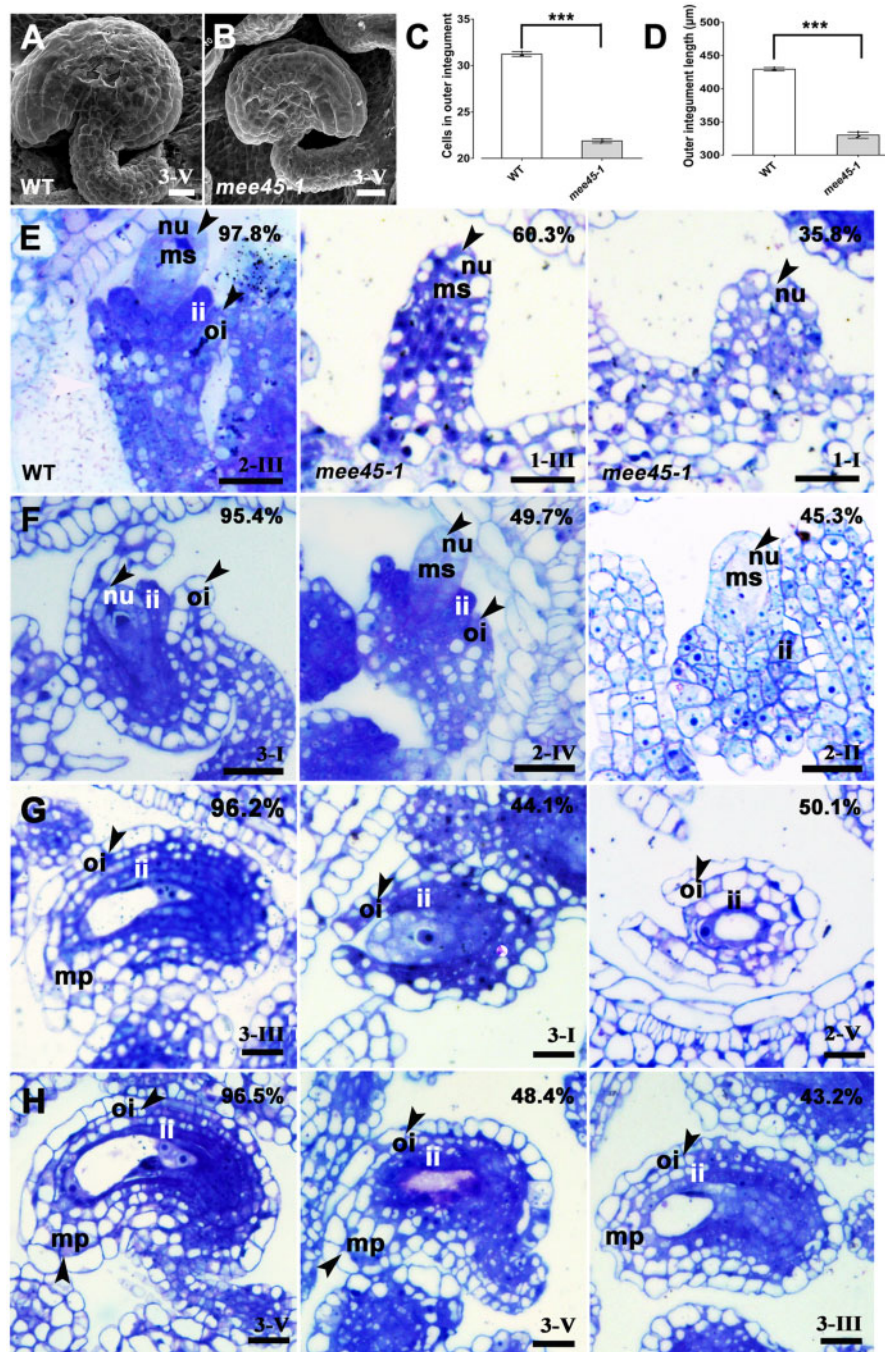
Figure 5 Ovules in the WT and *mee45-1* plants. A and B, Scanning electron microscopy of mature ovules (Stage 3-V) from WT (A) and *mee45-1* (B). C, Number of cells in the outer integument of mature ovules (Stage 3-V) from WT and *mee45-1* plants. D, Outer integument length of mature ovules from WT and *mee45-1* plants. The error bars in (C) and (D) represent the standard error of the mean, calculated from three sets of biological replicates. $^{***}P < 0.001$, compared to the WT (Col-0) (Student's t-test). E, Developing ovules from WT or *mee45-1* carpels at Stage 10. F, Developing ovule from WT or *mee45-1* carpels at stage 11. G, Developing ovule from WT or *mee45-1* carpels at stage 12. H, Developing ovule from WT or *mee45-1* carpels at Stage 13. Bars in (A), (B), and (E–H) = 100 μm. nu, nucellus; ms, megasporocyte; ii, inner integument; oi, outer integument; mp, micropyle.

the *mee45-1* mutant (Smyth et al., 1990; Guan et al., 2014), most WT ovules displayed the expanding inner and outer integuments identified as ovule Stage 2-III, ∼60% mutant ovules displayed their developing primordium at Stages 1-II, as well as roughly 35% mutant ovule primordia were at the earlier Stage 1-I (Figure 5E). Later in carpels at Stage 12, when WT ovules had fully developed inner and outer integuments enclosing the nucellus (ovule Stage 3-III), mutant ovules only displayed expanding inner and outer integuments at Stage 3-I or 2-V (Figure 5G). Although the

mature integuments of mutant ovules did enclose the nucellus eventually (by carpel Stage 13) and did thus exhibit the same pattern as the WT, mutant ovules were significantly smaller than WT ovules (Figure 5H).

MEE45 directly activates *ANT* expression in the ovule integument

To investigate the potential regulatory roles of MEE45 during ovule development and in seed size control, we performed deep sequencing of the transcriptome (RNA-seq) to identify genes regulated by MEE45. We identified 1,578 differentially expressed genes (DEGs) in *mee45-1* siliques compared to the WT (Supplemental Data Set S22), comprising 1,098 downregulated genes and 480 upregulated genes. The downregulated genes in *mee45-1*, which might be activated by MEE45, were enriched for functional annotations related to phytohormone metabolic processes, seed development, fatty acid biosynthetic processes, and environmental responses (Supplemental Figure S13A).

Our transcriptome analysis showed that the *ANT* gene is downregulated in *mee45-1* siliques compared to the WT (Supplemental Figure S13, A and B). *ANT* was previously demonstrated to maternally control seed size by promoting cell proliferation in ovule integument (Elliott et al., 1996; Klucher et al., 1996; Li and Li, 2015). To determine whether *ANT* functions downstream of *MEE45* in regulating the development of ovule integument, we examined *ANT* transcript levels in the mature ovules of WT and *mee45-1* plants, as well as from *mee45-1 MEE45pro:MEE45* and *MEE45pro:MEE45* (in Col-0) transgenic plants. *ANT* transcript levels were strongly diminished in the mature ovules of the *mee45-1* mutant (Supplemental Figures S13C and S14), returned to WT levels in *mee45-1 MEE45pro:MEE45* ovules, and significantly higher in *MEE45pro:MEE45* ovules compared to those in the WT (Supplemental Figure S14). We further analyzed the expression pattern of *ANT* by determining the fluorescence accumulation pattern of a yellow fluorescent protein (*YFP*) construct driven by the *ANT* promoter (*ANTpro:YFP*) in mature ovules of WT and the *mee45-1* mutant (Figure 6, A and B). Compared to the WT, YFP fluorescence was severely reduced in the mature ovule integuments of *mee45-1* plants, suggesting that MEE45 promotes *ANT* expression in the ovule integument.

To investigate whether MEE45 acts as a direct regulator of *ANT* transcription, we performed chromatin immunoprecipitation (ChIP) followed by quantitative PCR (qPCR; ChIP-qPCR) experiments using ovules from *35Spro:MEE45-GFP* lines. We saw an enrichment for the P1 fragment of the *ANT* promoter (-775 bp to -504 bp relative to the transcription start site, Figure 6D), which contained the potential binding site for B3-type transcription factors CATGCA (-628 bp to -623 bp). Electrophoretic mobility shift assays (EMSAs) revealed that MEE45 binding to the P1 fragment of the *ANT* promoter was completely abolished when we mutated the CATGCA motif to ACCTAC (Figure 6E). Together, these data strongly suggest that MEE45 directly binds to the predicted CATGCA motif of the *ANT* promoter. Furthermore, *YFP* reporter constructs driven by the *ANT* promoter with a mutated version of the MEE45-binding site (CATGCA to ACCTAC) showed a strong reduction of YFP fluorescence in transgenic ovule integuments compared to a construct driven by the native *ANT* promoter (Figure 6, A and C). These results support the hypothesis that MEE45 functions as a direct regulator of *ANT* transcription in the ovule integument, specifically through its binding at the *ANT* promoter.

MEE45 controls seed size by activating the expression of its target gene *ANT*

Previous studies revealed that loss-of-function *ant* mutants have defective ovules that fail to form integuments or female gametophytes (Klucher et al., 1996). To investigate the genetic relationship between *MEE45* and *ANT* in the control of ovule development and seed size, we identified a previously unexamined *ant* mutant with a T-DNA insertion in the 3′-untranslated region of the *ANT* locus (Supplemental Figure S15A). We refer to this new allele as *ant-T*. *ANT* transcript levels in mature ovules of the *ant-T* mutant were significantly reduced compared to those of the WT (Supplemental Figure S15B). Unlike published loss-of-function *ant* mutants, *ant-T* ovules produced functional female gametophytes and generated smaller seeds with normal seed germination and viability rates compared to the WT (Supplemental Figures S2 and S15, C, D, G, and H; Supplemental Data Sets S2, S4, S23, and S24), indicating that *ant-T* is a knockdown allele.

The small-seed phenotype seen in *ant-T* was completely rescued by the introduction of a *35Spro:ANT* transgene. The same *35Spro:ANT* transgene resulted in the production of significantly oversized seeds when introduced in the WT background (Supplemental Figure S15, E–H; Supplemental Data Sets S23 and S24). Compared to ovule development in the WT, *ant-T* ovule primordia appeared to form and enlarge normally, but integument initiation was delayed (Supplemental Figure S16, A–C). Although both the inner and outer integuments eventually enclosed the nucellus, mature ovules were smaller in *ant-T* compared to WT ovules (Supplemental Figure S16D), a phenotype shared with the *mee45-1* mutant (Figure 5H). Therefore, *ant-T* can be classified as a new knock-down mutant with milder phenotypes than previously reported *ant* alleles.

We then generated *mee45-1 ant-T* double mutant plants through genetic crossing and discovered that their seed size and weight did not differ from those of the *ant-T* mutant, but were significantly smaller than those of the *mee45-1* mutant (Figure 6, F–I, L, and M; Supplemental Data Sets S25 and S26). These results indicate that *ant-T* is epistatic to *mee45-1* for the seed size phenotype. We also found that the *ant-T* mutant suppressed the seed size increase that we had observed earlier in *MEE45*-overexpressing transgenic lines (Figure 6, J–M; Supplemental Figure S17; Supplemental Data Sets S25 and S26). These genetic results demonstrate
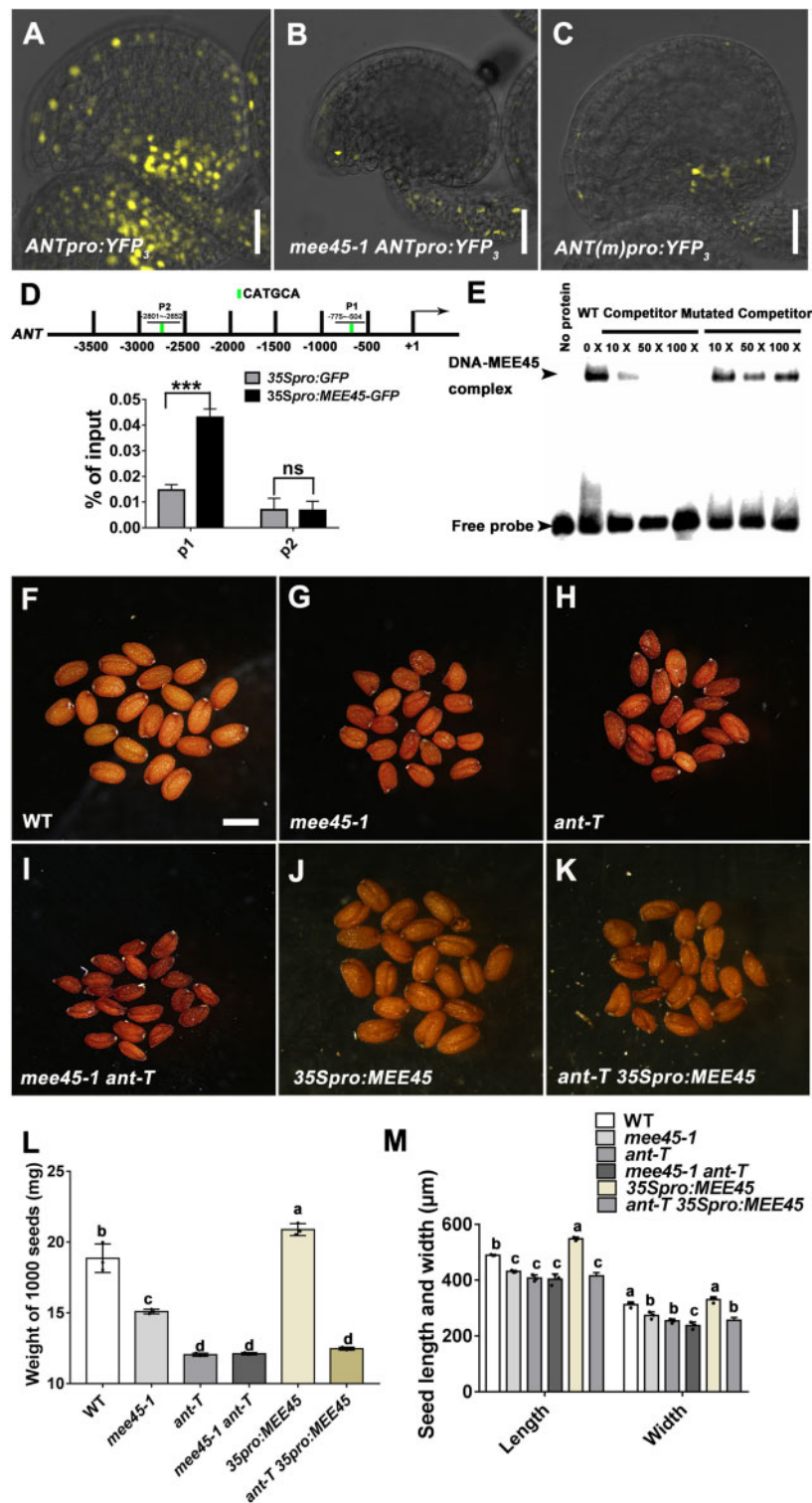
Figure 6 MEE45 controls seed size by directly activating *ANT* expression. A and B, Expression pattern of *ANT* from *ANTpro:YFP₃* in mature ovules of WT (A) and *mee45-1* (B). C, Expression pattern of *ANT* from *ANTpro:YFP₃* in mature WT ovules. Bars = 50 μm. D, ChIP-qPCR of the *ANT* promoter using an anti-GFP antibody in mature ovules of *35Spro:MEE45-GFP* transgenic lines, using *35Spro:GFP* ovules as negative control. MEE45 binds to region P1. The error bars represent the standard error of the mean, calculated from three sets of biological replicates. [***]$P < 0.001$, ns, not significant, compared to the WT (Col-0) (Student's *t*-test). E, Direct interaction between MEE45 and the *ANT* promoter, as determined by EMSA. The arrows indicate the position of the shifted bands and the free probe, respectively. F–K, Mature dry seeds of the WT (F), *mee45-1* (G), *ant-T* (H), *mee45-1 ant-T* double mutants (I), *35Spro:MEE45* (J), and *ant-T 35Spro:MEE45* (K) plants. Bar = 500 μm. L, Average seed mass per 1,000 seeds of the indicated genotypes. M, Average seed length and width of the indicated genotypes. The error bars in (L) and (M) represent the standard error of the mean, calculated from three sets of biological replicates. One-way ANOVA and Tukey's multiple comparison tests were performed. Statistically significant differences are indicated by different lowercase letters ($P < 0.05$).

that *ANT* functions as a direct target of MEE45 in the maternal control of seed size.

MEE45 controls seed size by inducing *YUC*-mediated auxin biosynthesis in the ovule integument

YUCs are auxin biosynthetic genes, and our transcriptomic analysis showed *YUC1*, *YUC2*, *YUC4*, *YUC5*, and *YUC10* among significantly downregulated DEGs in the *mee45-1* mutant compared to the WT (Supplemental Figure S13, A and B). We confirmed the significantly differential expression of *YUC* genes in the mature ovules of WT and *mee45-1* mutant plants using qPCR (Supplemental Figure S13C). We further characterized the expression pattern of *YUC4*, whose differential expression was the most pronounced among differentially expressed *YUCs*, in the ovules of the *mee45-1* mutant and in *MEE45*-overexpressing lines (Figure 7, A–C) by introducing a *GFP* reporter construct under the control of the *YUC4* promoter. Compared to the WT, fluorescence from the *YUC4pro:GFP* reporter was severely reduced in the integuments of *mee45-1* mutant ovules. In contrast, the GFP signal was significantly stronger in ovule integuments of *MEE45*-overexpressing lines relative to the WT. Moreover, the small-sized seed phenotype in the *mee45-1* mutant was completely rescued when we expressed the *YUC4* gene under the control of the *MEE45* promoter (Figure 7, D–F, L, and M; Supplemental Data Sets S27 and S28). Thus, MEE45 promotes *YUC*-mediated auxin biosynthesis in the integument.

As the *mee45-1* mutant displayed decreased expression of multiple auxin biosynthetic genes in ovules, we measured auxin content in the mutant and WT backgrounds. The total IAA content in *mee45-1* siliques was significantly lower than in WT siliques (Supplemental Figure S18A). We further evaluated the fluorescence derived from the auxin reporter *DR5:GFP* in ovules of the *mee45-1* mutant and *MEE45*-overexpressing lines. Similar to *YUC4* expression, fluorescence from the *DR5:GFP* reporter was severely reduced in *mee45-1* mutant ovules, but was significantly increased in ovules of *MEE45*-overexpressing lines compared to the WT (Supplemental Figure S18, C–E). Collectively, these results indicate that the mutation of *MEE45* leads to decreased auxin levels and a localized downregulation of auxin response in ovules.

We hypothesized that a lack of auxin accumulation in ovule integument might cause the observed small seed size phenotype of the *mee45-1* mutant. To test this hypothesis, we expressed *YUC4* specifically in the integument of the *mee45-1* mutant by using the aforementioned *INO* promoter (Supplemental Figure S18, B, F, and G). The *INOpro:YUC4* transgene caused a strong and significant increase of seed size in the *mee45-1* mutant, even producing oversized seeds as compared to the WT (Figure 7, D, E, G, L, and M; Supplemental Data Sets S27 and S28). Moreover, expression of the *INOpro:YUC4* transgene in the WT background produced significantly oversized seeds compared to the WT control (Figure 7, D, H, L, and M; Supplemental Data Sets

S27 and S28). These findings indicate that the small seed size in the *mee45-1* mutant apparently results from an auxin deficiency in the integument and support the idea that auxin biosynthesis in ovule integument contributes to the control of seed size.

Overexpression of *MEE45* resulted in oversized seeds (Figure 7, D, I, L, and M; Supplemental Data Sets S27 and S28). However, mutations of the *YUC* genes in the *yuc1 yuc4 yuc10* triple mutant largely suppressed the seed size increase caused by *MEE45* overexpression, displaying seeds with no significant difference in size or weight compared to the *yuc1 yuc4 yuc10* triple mutant, which itself had significantly smaller seeds than the WT (Figure 7, I–M; Supplemental Figure S17; Supplemental Data Sets S27 and S28). Together, these observations provide strong evidence that MEE45 controls seed size by increasing auxin biosynthetic capacity in ovule integuments.

## A MEE45–ANT pathway regulates auxin biosynthesis in the ovule integument

Given our findings that expression of both *ANT* and *YUC* genes requires MEE45, and our demonstration of *ANT* as a binding and transcriptional activation target of MEE45, we further tested whether *YUC* genes may act downstream of MEE45–ANT during integument development. Most *YUC* transcript levels were significantly lower in *ant-T* mutant ovules compared to the WT (Figure 8A). In agreement, *ant-T* mutant siliques had significantly reduced total IAA content compared to the WT (Supplemental Figure S18A). Furthermore, fluorescence of the *YUC4pro:GFP* reporter was significantly reduced in ovule integuments of the *ant-T* mutant (Figure 8, C and D).

To further investigate whether ANT directly interacts with the *YUC4* promoter to regulate *YUC4* expression, we performed a ChIP-qPCR assay using mature ovules from *35Spro:ANT-GFP* lines (Figure 8B). Of the fragments (P1–P7) covering the entire presumptive 1,850 bp *YUC4* promoter region, only the P1 and P7 fragments were strongly enriched by immunoprecipitation with the anti-GFP antibody, respectively, spanning the regions from −210 bp to −41 bp and from −1,848 bp to −1,528 bp. Each P1 and P7 fragments had one AP2 repeat (ANT-AP2R2) binding site, which is bound by ANT in vitro (Nole-Wilson and Krizek, 2000). These results suggest that ANT binds to the *YUC4* promoter and activates its transcription.

Moreover, expressing *YUC4* under the control of the *INO* promoter (*INOpro:YUC4*) rescued the small seed size seen in the *ant-T* mutant, even leading to seeds that were oversized compared to the WT, and showed no significant difference with the seeds of WT plants carrying the *INOpro:YUC4* transgene (Figure 8, E–J; Supplemental Figure S18H; Supplemental Data Sets S29 and S30). Intriguingly, *MEE45* overexpression in the *ant-T* background did not cause a similar extent of *YUC4* expression induction as in the WT background: we detected the weak expression of *YUC4* in ovule integuments from *MEE45*-overexpressing *ant-T* lines, but this
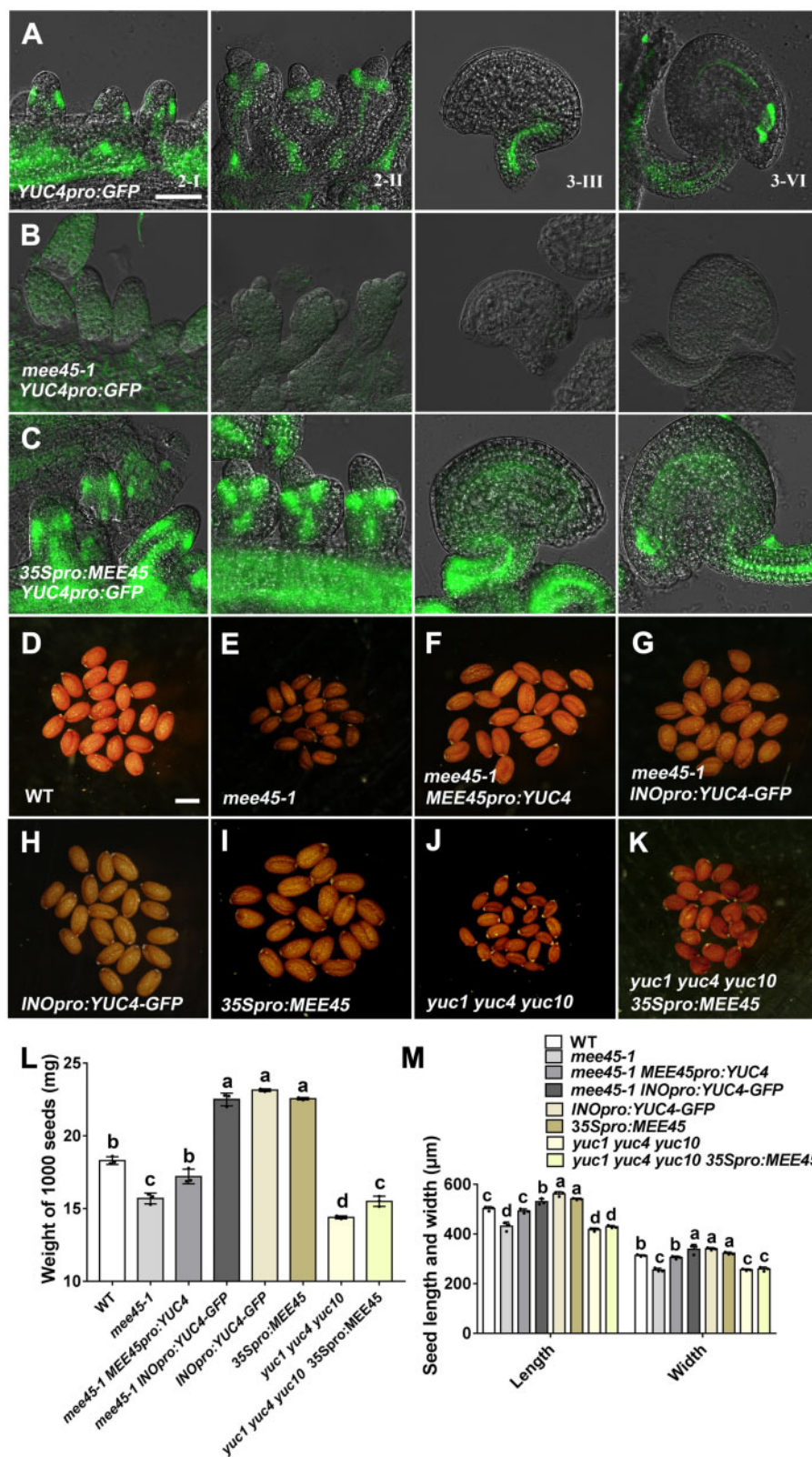
Figure 7 Seed size in *mee45-1* is reduced due to reduced auxin biosynthesis capacity in the ovule integument. A–C, Expression pattern of *YUC4* in ovules at the 2-I, 2-II, 3-III, and 3-VI (mature ovule) stages of *YUC4pro:GFP* (A), *mee45-1 YUC4pro:GFP* (B) and *35Spro:MEE45 YUC4pro:GFP* (C) transgenic plants. Bar = 50 μm. D–K, Mature dry seeds of the WT (D), *mee45-1* (E), *mee45-1 MEE45pro:YUC4* (F), *mee45-1 INOpro:YUC4-GFP* (G), *INOpro:YUC4-GFP* (H), *35Spro:MEE45* (I), *yuc1 yuc4 yuc10* triple mutants (J), and *yuc1 yuc4 yuc10 35Spro:MEE45* (K) plants. Bar = 500 μm. L, Average seed mass per 1,000 seeds of the indicated genotypes. M, Average seed length and width of the indicated genotypes. The error bars in (L) and (M) represent the standard error of the mean, calculated from three sets of biological replicates. One-way ANOVA and Tukey's multiple comparison tests were performed. Statistically significant differences are indicated by different lowercase letters ($P < 0.05$).
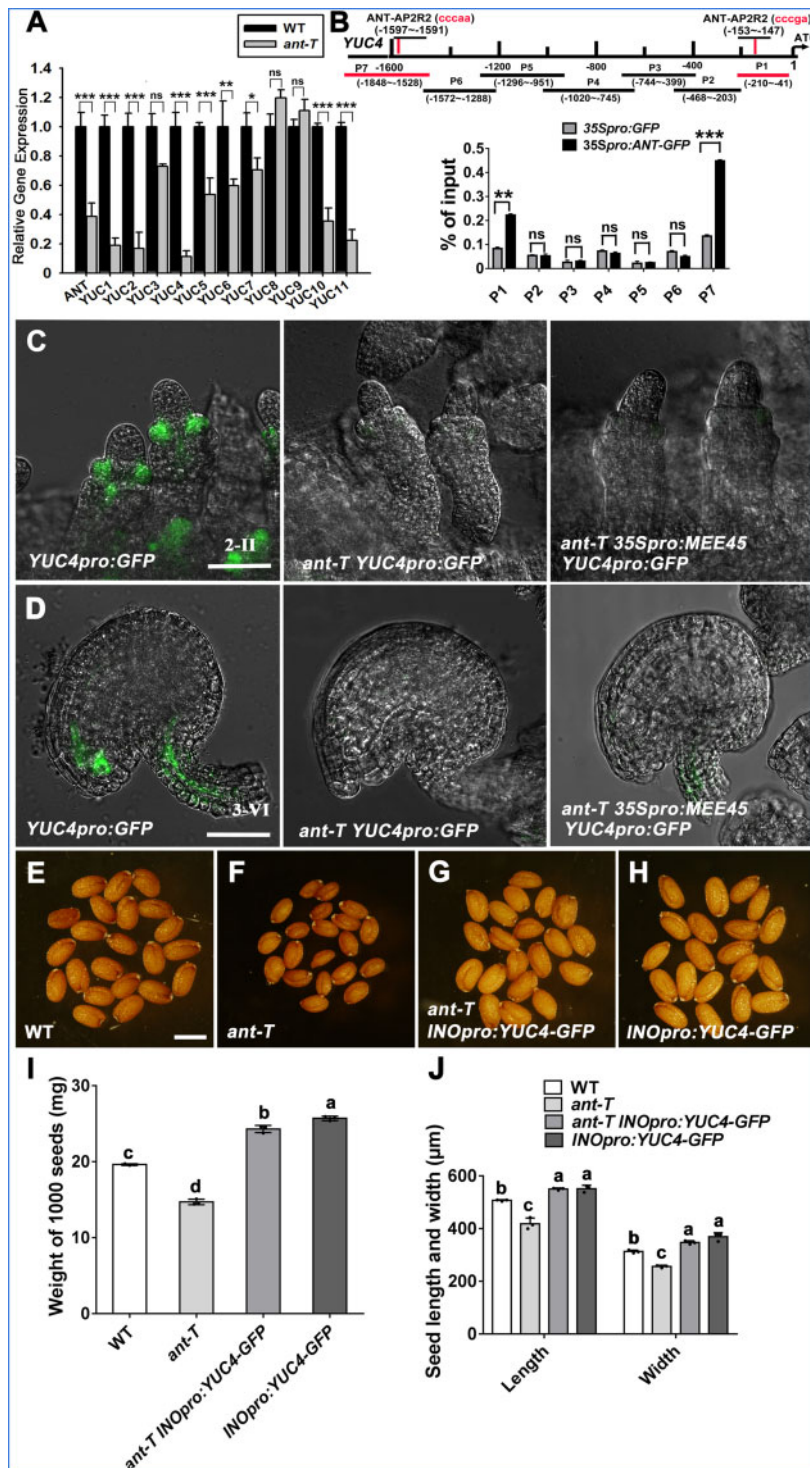
Figure 8 ANT activates auxin biosynthesis in the ovule integument. A, Relative expression levels of *YUC* genes in mature ovules of WT and *ant-T*. The error bars represent the standard error of the mean, calculated from three sets of biological replicates. $^{***}P < 0.001$, $^{**}P < 0.01$, $^{*}P < 0.05$, ns, not significant, compared to the WT (Col-0) (Student's *t*-test). B, ChIP-qPCR of the *YUC4* promoter using an anti-GFP antibody in the mature ovules of *35Spro:ANT-GFP* transgenic plants, using ovules from *35Spro:GFP* transgenic plants as negative control. ANT binds to regions P1 and P7. The error bars represent the standard error of the mean, calculated from three sets of biological replicates. $^{**}P < 0.01$, $^{***}P < 0.001$, ns, not significant, compared to the WT (Col-0) (Student's *t*-test). C, Expression pattern of *YUC4* in stage 2-II ovules of *YUC4pro:GFP*, *ant-T YUC4pro:GFP*, and *ant-T YUC4pro:GFP 35Spro:MEE45* transgenic plants. D, Expression pattern of *YUC4* in stage 3-VI (mature) ovules of *YUC4pro:GFP*, *ant-T YUC4pro:GFP* and *ant-T YUC4pro:GFP 35Spro:MEE45* transgenic plants. Bars = 50 μm. E–H, Mature dry seeds of the WT (E), *ant-T* (F), *ant-T INOpro:YUC4-GFP* (G) and *INOpro:YUC4-GFP* (H) plants. Bar = 500 μm. I, Average seed mass per 1,000 seeds of the indicated genotypes. J, Average seed length and width of the indicated genotypes. The error bars in (I) and (J) represent the standard error of the mean, calculated from three sets of biological replicates. One-way ANOVA and Tukey's multiple comparison tests were performed. Statistically significant differences are indicated by different lowercase letters ($P < 0.05$).
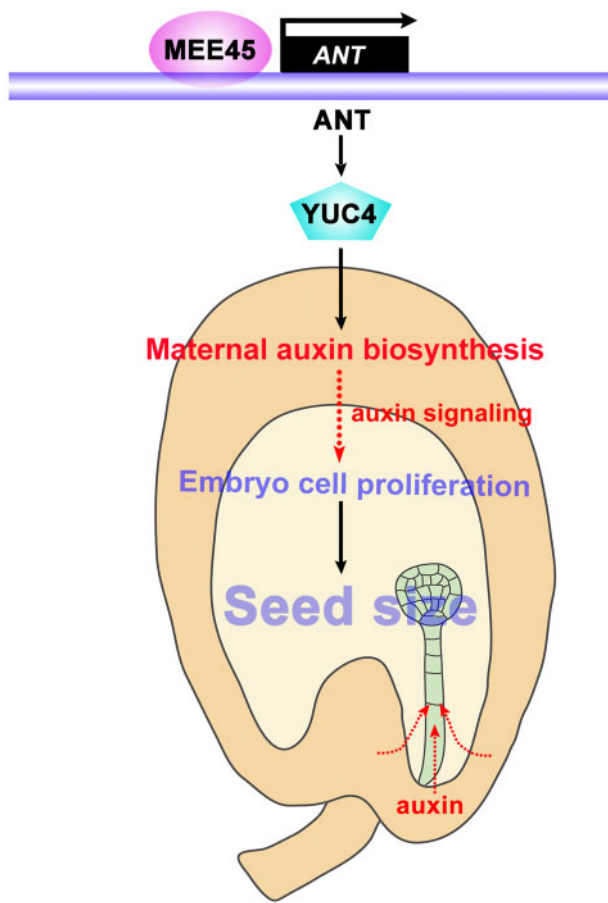
Figure 9 A working model for how a MEE45–ANT pathway in maternal tissues modulates auxin biosynthesis and seed size in Arabidopsis. The integuments are maternal tissues that surround the ovule, setting an upper limit for the embryo to grow and impacting the final seed size. In the ovule integument, MEE45 positively regulates *ANT* transcription by directly binding to the *ANT* promoter region, and ANT in turn directly interacts with the *YUC4* promoter to activate *YUC4* expression. MEE45 and ANT function in the same genetic pathway to regulate the expression of *YUC4*, thereby mediating maternal auxin biosynthesis. Auxin biosynthesized in the maternal ovule integument may generate a signal received by embryos or move directly into the embryos to affect their development, and further determines the seed size.

level did not differ from the *YUC4* level in the *ant-T* mutant (Figure 7, A and C; Figure 8, C and D). These results suggest that a MEE45–ANT pathway activates the expression of *YUC4*, thereby promoting the auxin biosynthesis capacity of cells in the ovule integument (Figure 9).

Discussion

Integuments are maternal tissues that surround the ovule and form the seed coat after fertilization. Integuments also provide the cavity for the growth of the embryo and the endosperm, and set an upper limit to seed size (Fang et al., 2012; Xia et al., 2013; Du et al., 2014). Here, we show that MEE45 is essential for the proliferation of integument cells and size control of mature ovules, which also controls

embryo size in the limited space within seed coats. These findings indicate that MEE45 acts as a regulator in maternal tissues, and the regulation of ovule integument development by MEE45 clearly influences the determination of final seed size.

Several signaling pathways have been identified that control seed size in Arabidopsis and rice, including for example the IKU pathway, which integrates abscisic acid, brassinosteroids, and cytokinin signaling to control seed size by regulating endosperm development (Li et al., 2019). Seed size is also mediated by the growth of maternal tissues. Previous studies have suggested that maternal tissues contribute to seed size control: mutants with maternal tissue defects such as *da1* and *ap2* affect seed size through alternation of cell proliferation and/or expansion in ovule integuments (Li et al., 2008; Adamski et al., 2009). These studies have established that the effects on seed size of the *da1* and *ap2* mutants result from the genotypes of the maternal tissues, rather than the genotype of the zygotic tissues.

Transcriptional regulation is central throughout the plant life cycle, including during seed development. Several transcription factors have been identified as regulators of seed size. The Arabidopsis *ANT* gene encodes an AP2-like transcription factor and was identified as a regulator of integument initiation and ovule development, as well as organ growth (Elliott et al., 1996; Klucher et al., 1996; Mizukami and Fischer, 2000). *ant* mutants exhibit defects in ovule development with abnormal initiation of integuments, whereas overexpressing *ANT* produces oversized seeds resulting from a promotion of excessive cell proliferation in integuments. Thus, ANT is a transcription factor that maternally controls seed size. Another Arabidopsis regulator of cell proliferation and expansion is *ARF2*, which encodes a plant-specific B3 superfamily transcription factor involved in auxin signaling (Li et al., 2004). ARF2 acts maternally to control seed growth by restricting integument cell proliferation (Schruff et al., 2006). Mutation of *ARF2* causes phenotypes including increased seed and organ size, abnormal flower morphology, and enhanced seed abortion (Schruff et al., 2006). A previous study showed that ARF2 binds to the *ANT* promoter and negatively regulates its transcription in seedling leaves and stems, as well as in developing siliques (Meng et al., 2015).

Similar to ARF2, another two Arabidopsis B3 domain transcription repressors, NGATHA-LIKE 2 (NGAL2; also named SUPPRESSOR OF DA1) and DEVELOPMENT-RELATED PcG TARGET IN THE APEX4 (also named NGAL3) were identified to act redundantly to maternally regulate seed size by limiting cell proliferation in integuments (Zhang et al., 2015). NGAL2 binds to the promoter of *KLUH* and negatively regulates its expression. In this study, we identified MEE45 as a B3 domain transcription factor that maternally regulates seed size. We show that MEE45 directly induces *ANT* expression in the ovule, which promotes integument cell proliferation and thereby regulates seed size. MEE45 and ARF2 both have *ANT* as their common target, but these

two B3 domain transcription factors exert opposite transcriptional regulatory functions and therefore cause inverse effects on seed size. These findings highlight the multiple signaling pathways that function upstream of *ANT* for the maternal control of seed development. It will be interesting to further characterize how MEE45 and potentially several other B3 domain transcription factors differentially regulate maternal control of seed development via *ANT*, and such work may reveal the signaling components and perhaps environmental or cellular factors that function further upstream of these B3 domain transcription factors in specifying seed size.

Auxin controls cell division and cell expansion (Vandenbussche and Van Der Straeten, 2004; Leyser, 2005; Yao et al., 2019) Similar to ARF2 in Arabidopsis, BnARF18 in rapeseed (*Brassica napus*) represses auxin-responsive genes to maternally control seed size by restricting cell expansion (Liu et al., 2015a). Overexpression of *ARF19* in purging nut (*Jatropha curcas*, an oilseed crop) results in an increased seed size (Sun et al., 2017). A recent study showed that ARF6 and ARF8 may mediate auxin responses in maternal tissues and contribute to seed development in Arabidopsis (Yao et al., 2019). Auxin signaling thus modulates maternal regulation of seed development and seed size. However, our current understanding of how auxin biosynthesis or accumulation controls seed size is limited. In this study, we show that the expression of auxin biosynthesis gene *YUC4* in the ovule is positively regulated by ANT, whose expression is in turn directly induced by MONOPTEROS (also named ARF5) in floral primordium initiation (Yamaguchi et al., 2013). These data suggest a positive feedback regulation between ANT and auxin activity in the ovule, which may contribute to seed size control.

Previous studies have shown that maternally produced auxin in the integument after fertilization affects early embryo development (Robert et al., 2018). Our results provide new insights into the mechanisms by which auxin biosynthesis in integuments contributes to the regulation of seed development and final seed size. It will be intriguing to explore whether auxin biosynthesized in maternal integuments generates a signal received downstream by embryos; alternatively, auxin may move directly from maternal cells into embryos and thereby affect their development (Figure 9). Fertilization of the central cell is known to lead to the production of auxin in the endosperm, from which auxin is then exported to maternal tissues to drive seed coat development (Figueiredo et al., 2015). A defect in auxin export from the zygotic tissue to maternal tissues results in abnormal growth of maternal tissues and leads to further reduced seed size (Figueiredo et al., 2016). Together with these published findings, our results deepen our understanding of the mechanisms that regulate local auxin biosynthesis, signaling, and activity to coordinate the development of ovule integuments, embryos, and the endosperm, ultimately contributing to seed size control.

In conclusion, our results demonstrate that a MEE45–ANT pathway maternally regulates seed size. This pathway controls seed growth through the modulation of auxin biosynthesis genes in ovule integuments, tissues known to function as central hubs for the development of both maternal and zygotic tissues in plant reproduction (Figure 9) (Li and Li, 2016). These results improve our understanding of the mechanisms underlying maternal tissue-mediated regulation of seed size. Manipulating MEE45 and/or related pathways and components in crops may enable new technologies to increase seed yield in crop production.

Material and Methods

Plant materials and growth conditions

All mutants and marker lines used in this study were in the Arabidopsis (*A. thaliana*) Col-0 accession. The T-DNA insertion lines *mee45-1* (SALK_031530), *mee45-2* (SALK_038324), *mee45-3* (CS801014), and *ant-T* (SALK_022770) were obtained from the Arabidopsis Biological Resource Center. The lines *YUC4pro:GFP* (Cheng et al., 2013), *35Spro:GFP* (Su et al., 2020), and the *yuc1 yuc4 yuc10* triple mutant (Cheng et al., 2006) have been described previously. We generated the *mee45-1 ant-T* double mutant by crossing *mee45-1* with *ant-T*, and used F_3 homozygous plants for imaging and measurements.

We surface sterilized all seeds before sowing them on 0.8% (w/v) agar solid medium (half-strength Murashige and Skoog (MS) medium, 1% sucrose, pH 5.7). After breaking dormancy at 4°C for 2 days in the dark, we allowed seeds to germinate and seedlings to grow under long-day conditions (16-h light/8-h dark) with white light 120 μmol/m^2/s at 22°C for 10 days, before transplanting individual seedlings to soil for further growth.

Plasmid construction and plant transformation

We generated the *MEE45pro:MEE45*, *MEE45pro:YUC4* constructs using the GreenGate system (Lampropoulos et al., 2013). We PCR-amplified a 1,970-bp fragment of the *MEE45* promoter from Col-0 genomic DNA using 2× Phanta Max Master Mix (Vazyme, Nanjing, China ; P515-01), digested the resulting PCR products with *Bsa*I, and then ligated the purified digested products into the *Bsa*I site of the empty entry vector pGGA000 to yield a new promoter module. We amplified the *MEE45* and *YUC4* CDSs by PCR from Col-0 cDNAs, and ligated the PCR products at the *Bsa*I site of the empty entry vector pGGC000 to generate new CDS modules. We then strung the four modules (pGGB003, pGGD002, pGGF005, and pGGZ001) with the promoter module and the CDS modules described above.

We generated the *INOpro:MEE45-GFP*, and *INOpro:YUC4-GFP* constructs using the GreenGate system. We PCR-amplified a 2,012-bp fragment of the *INO* promoter from Col-0 genomic DNA, digested the resulting PCR products with *Bsa*I, and then ligated the purified digested products into the *Bsa*I site of the empty entry vector pGGA000 to yield a new promoter module. We amplified the *MEE45* and *YUC4*

CDSs by PCR from Col-0 cDNAs, and ligated the PCR products at the *Bsa*I site of the empty entry vector pGGC000 to generate new CDS modules. We then strung the four modules (pGGB003, pGGD001, pGGF005, and pGGZ001) with the promoter module and the CDS modules described above.

Following the same strategy, to generate the *RPS5Apro:amiRNA-MEE45* construct, the *MEE45* amiRNA was generated by PCR amplification with the combinations of primers shown in Supplemental Table S1. The amiRNA-*MEE45* construct was cloned into empty entry vector pGGC000 to generate a new module. We then strung the five modules (pGGA012, pGGB003, pGGD002, pGGF005, and pGGZ001) with the amiRNA module described above.

To generate the *gMEE45-GFP* construct, we PCR-amplified a 4,045-bp *MEE45* genomic fragment and inserted it into the pENTR entry vector, before recombination into the pMDC107 vector (Gateway system, Invitrogen, Carlsbad, CA, USA) through Gateway LR recombination.

To generate the *35Spro:MEE45* and *35Spro:ANT* constructs, we independently PCR-amplified the *MEE45* and *ANT* CDS from Col-0 cDNAs, digested the PCR products with *Sac*I and *Pst*I, and ligated the purified and digested fragments into the pCAMBIA1300 vector.

To generate the *35Spro:ANT-GFP* and *35Spro:MEE45-GFP* constructs, we independently PCR-amplified the *ANT* and *MEE45* CDSs from Col-0 cDNA, digested the PCR products with *Kpn*I/*Spe*I and *BamH*I/*Kpn*I, then ligated the purified and digested fragments into the pROK II-GFP vector.

To generate the *ANTpro:YFP$_3$* construct, we PCR-amplified a 2,019-bp DNA fragment of *ANT* genomic sequence upstream of the putative initiation codon and cloned in frame with *NLS-3×YFP* followed by a 35S terminator.

The primers used for plasmid construction are listed in Supplemental Table S1. The constructs were transformed into all genotypes using the floral dip method (Clough and Bent, 1998). Homozygous transgenic plants (T$_2$ generation) were used in this study.

Analysis of seed size and seed mass

To determine seed mass, we weighed 1,000 mature dry seeds in each replicate. All measurements were repeated 3 times. After capturing photographs with a stereomicroscope connected to a computer, we used ImageJ to measure the length and width of seeds. Three replicates were used for statistical analysis, and in each replicate, ∼30 seeds were examined.

Total RNA isolation and real-time qPCR analysis

Total RNA was extracted from the indicated tissue using Ultrapure RNA Kit (CWbiotech, Beijing, China). First-strand cDNAs were then synthesized by FastQuant RT Kit (Tiangen Biotech, Beijing, China). SYBR Green Real-time PCR Master Mix (Tiangen Biotech) was used for qPCR, according to the manufacturer's protocol. The SYBR Green Master mix was used to dilute each cDNA. For all samples, relative transcript levels were normalized to *TUBULIN2*, and all measurements

were carried out in three biological replicates. To determine expression values, we used the comparative C_T method. The primers used for qPCR analysis are listed in Supplemental Table S1.

Immunoblotting

To analyze MEE45 protein accumulation, total proteins were extracted from mature ovules of WT, *mee45-1*, *mee45-1 MEE45pro:MEE45* and *MEE45pro:MEE45* lines with extraction buffer (140 mM NaCl, 0.537 mM KCl, 0.2939 mM KH$_2$PO$_4$, 5 mM Na$_2$HPO$_4$, 0.01 mM EDTA, 0.05% NP-40, 5 mM DTT, 0.5 mM PMSF, 1× protease inhibitor cocktail). Samples were centrifuged at 4°C, at 12,000 r.p.m. for 60 min. The supernatant was then transferred to a new tube and used for gel electrophoresis. MEE45 protein was detected by immunoblot using anti-MEE45 antibody (1:1,000 dilution, polyclonal antibody produced by Abmart, using Arabidopsis MEE45 protein as antigen). ACTIN was detected by anti-ACTIN antibody (1:1,000 dilution, A01050; Abbkine Wuhan Shi, China) as loading control, followed by goat anti-rabbit (1:1,000 dilution, ZB-5301; ZSGB-BIO, Beijing, China) or goat anti-mouse (1:1,000 dilution, A0216; Beyotime, Shanghai, China) HRP-conjugated secondary antibody. Signal was visualized using a Universal Hood II (BIO-RAD, Hercules, CA, USA). Immunoblot experiments were repeated 3 times.

DIC microscopy and image processing

We observed embryo and endosperm development in cleared seeds using differential interference contrast (DIC) optics as previously described (Ohto et al., 2009). We cleared specimens with a chloralhydrate/glycerol/water (8:3:1) solution, and collected images on a DIC microscope connected to a computer for image capture.

Sectioning and cytological analysis

Siliques were cut at both ends and fixed in glutaraldehyde fixative under vacuum for 10 min. Siliques were then rinsed twice in 0.2 M phosphate buffer, pH = 7.0 before dehydration through a graded ethanol series: 10% (v/v with water), 30%, 50%, 70%, 95% (eosin added), and 100%, each time for 1 h. We incubated samples in propylene oxide for 1 h, followed by propylene oxide and epoxy (v/v 1:1) incubation overnight at room temperature. We then incubated the specimens with an epoxy resin accelerant for 2 days, changing the solution once a day. We finally embedded the specimens in the same solution at 42°C overnight, and then 60°C for 2 days. We used a Leica Microsystems RM2265 microtome to slice the specimens, followed by dyeing with 1% Toluidine Blue O. A stereomicroscope was used for image acquisition. Then, the sections were photographed with an Olympus BH-2 microscope equipped with an Olympus digital camera.

Scanning electron microscopy

Mature ovules were immersed in glutaraldehyde fixative for 20 h at room temperature and then rinsed 5 times for 20 min each in phosphate-buffered saline (PBS) buffer.

Following immersion in osmium tetroxide for 5 h, we rinsed specimens in PBS buffer 3 times for 20 min each. The specimens were then dehydrated with a graded ethanol series (45%, 55%, 70%, 85%, 95%, and 100%). Critical-point drying was accomplished under liquid carbon dioxide. The specimens were mounted on stubs, sputter-coated with palladium gold, then examined with a scanning electron microscope (JSM-6610; JEOL, Tokyo, Japan).

Transcriptome analysis

We collected siliques 3 days after pollination from Col-0 and *mee45-1* plants for RNA-seq analysis as three independent biological replicates per genotype. The libraries were constructed with NEBNext Ultra RNA Library Prep Kit for Illumina and checked on an Agilent 2100 Bioanalyzer. The libraries were then sequenced on a HiSeq 2500 platform (Illumina, San Diego, CA, USA). After removing adapters, reads with Ns, and low-quality reads, clean reads were mapped to the *A. thaliana* genome (version: Arabidopsis Information Resource [TAIR] 10) with TopHat2 with default parameters (Kim et al., 2013). Fragment per kilobase of exon per million reads mapped was used to estimate transcript abundance. Genes with at least two-fold change and a false discovery rate <0.1 were considered DEGs.

Observation of ovules development

Developing ovules were fixed in glutaraldehyde fixative under vacuum for 30 min, then incubated overnight at 4°C. The specimens were dehydrated in a graded ethanol series (30%, 40%, 50%, 60%, 70%, and 100%) for 30 min each. We cleared specimens with benzoate and benzyl alcohol (v/v 2:1) for 2 h, and acquired images with a Zeiss 880 laser scanning microscope with 488 nm laser excitation and 505–550 nm emission spectra.

GUS staining

Specimens (*CYCB1;1pro:GUS, mee45-1 CYCB1;1pro:GUS*) were stained in GUS staining solution (1 mM 5-bromo-4-chloro-3-indolyl-b-D-glucuronic acid, 100 mM Na$_3$PO$_4$ buffer, 3 mM each K$_3$Fe(CN)$_6$/K$_4$Fe(CN)$_6$, 10 mM EDTA, and 0.1% Nonidet P-40) and incubated at room temperature for 5 h. After GUS staining, chlorophyll was removed in 70% ethanol.

Fluorescence analysis

We acquired confocal laser-scanning micrographs of ovules and embryos with a Zeiss 880 laser scanning microscope. For GFP and YFP detection, we used 488 and 514 nm laser excitation, 505–550 nm, and 530–600 nm emission spectra for each respective excitation. We acquired, analyzed, and exported images with the help of the Zeiss ZEN software.

ChIP analysis

We performed ChIP on mature ovules collected from *35Spro:MEE45-GFP, 35Spro:ANT-GFP* and *35Spro:GFP* lines using an EZ ChIP Kit (Millipore, Burlington, MA, USA), according to previously described protocols (Su et al., 2020) with minor modifications. Bioruptor was used for sonication (250W, 20%, repeat 4–6 times; sonication buffer: 1 mL SDS Lysis buffer with 5 µL Protease inhibitor cocktail II). We used anti-GFP antibody (1:500 dilution, SAB5300167; Sigma St Louis, MO, USA) to precipitate chromatin. *35Spro:GFP* lines were used as negative controls. For each ChIP assay, we performed three biological and three technical repeats. All primer sequences used for ChIP assays are listed in Supplemental Table S1.

EMSA

We performed EMSA as previously described (Su et al., 2020). We largely followed the instructions supplied with the Light Shift Chemiluminescent EMSA kit (Thermo Scientific, Waltham, MA, USA). To purify the MEE45-GST fusion protein, we cloned the *MEE45* CDS into the pGEX-4T vector, and produced the protein in *Escherichia coli* BL21 (DE3), followed by purification with Glutathione Sepharose 4B beads (GE Healthcare, Chicago, IL, USA). Biotin-labeled probes were commercially synthesized. The WT sequence CATGCA corresponding to the −628 bp to −623 bp region of the *ANT* promoter, which contains the MEE45-binding site, was replaced with ACCTAC in the mutated probe.

Free IAA measurements

We harvested siliques 3 days after pollination from Col-0, *mee45-1*, and *ant-T* plants for free IAA measurements, using three independent biological replicates per genotype. Free IAA measurements were performed as previously described (Wang et al., 2015).

Seed germination and viability analysis

High-temperature and high-moisture conditions were used to evaluate Arabidopsis seed vigor. We tested seed germination or seed viability as previously described (Li et al., 2017). Seeds used to measure vigor were placed in a seed aging chamber at 83% relative humidity, 42°C for 72 h to accelerate aging, and then dried at room temperature for 24 h. Seeds treated with or without aging were surface-sterilized before sowing on 0.8% (w/v) agar solid half-strength MS medium for germination at 22°C. Germination was determined every 12 h. Three replicates were used for statistical analysis. In each replicate, 50 seeds were examined.

Accession numbers

Gene sequence data form this article can be found in the TAIR under the following accession number: *MEE45* (At4g00260), *ANT* (At4g37750), *MINI3* (At1g55600), *IKU1* (At2g35230), *IKU2* (At3g19700), *SHB1* (At4g25350), *YUC1* (At4g32540), *YUC2* (At4g13260), *YUC3* (At1g04610), *YUC4* (At5g11320), *YUC5* (At5g43890), *YUC6* (At5g25620), *YUC7* (At2g33230), *YUC8* (At4g28720), *YUC9* (At1g04180), *YUC10* (At1g48910), and *YUC11* (At1g21430). RNA-seq data discussed in this study have been deposited at the National Center for Biotechnology Information Gene Expression Omnibus under accession number GSE156491. All source data are provided with this article.

Supplemental data

The following materials are available in the online version of this article.

Supplemental Figure S1. Characterization and function of the *MEE45* gene.

Supplemental Figure S2. Seed germination and viability of the WT, *mee45-1* and *ant-T*.

Supplemental Figure S3. Mature ovules and embryo development in WT, *mee45-2* and *mee45-3* mutants.

Supplemental Figure S4. Relative expression of MEE45 in mature ovules of the indicated genotypes.

Supplemental Figure S5. The mature embryos of WT, *mee45-1*, *mee45-1 MEE45pro:MEE45* and *MEE45pro:MEE45* plants.

Supplemental Figure S6. Endosperm development in WT and *mee45-1* seeds.

Supplemental Figure S7. Relative expression of *MEE45* in different organs.

Supplemental Figure S8. The phenotypes of leaves, flowers, and siliques in *mee45-1* mutants compared to WT plants.

Supplemental Figure S9. Reciprocal cross experiments between the WT and *mee45-2*.

Supplemental Figure S10. Reciprocal cross experiments between the WT and *mee45-3*.

Supplemental Figure S11. *MEE45* Expression in the *INOpro:MEE45-GFP* and *mee45-1 INOpro:MEE45-GFP* transgenic lines.

Supplemental Figure S12. Cell proliferation indicated by *CYCB1;1pro:GUS* expression in the mature ovules of the WT and *mee45-1* mutant.

Supplemental Figure S13. Functional enrichment and gene expression analysis of RNA-seq data in the WT and *mee45-1* mutants.

Supplemental Figure S14. Relative expression of *ANT* in mature ovules of the indicated genotypes.

Supplemental Figure S15. Characterization and function of the *ANT* gene.

Supplemental Figure S16. Ovule development in the WT and *ant-T* plants.

Supplemental Figure S17. Relative expression of *MEE45* in mature ovules of the indicated genotypes.

Supplemental Figure S18. IAA content and expression of *YUC4* in mature ovules of the indicated genotypes.

Supplemental Table S1. Primers used for qPCR, ChIP-qPCR, and constructions of expression vectors

Supplemental Data Set S1. Figure 1I data: Seed mass per 1,000 seeds for the indicated genotypes.

Supplemental Data Set S2. Figure 1J data: Seed length and width for the indicated genotypes.

Supplemental Data Set S3. Supplemental Figure S2G data: Number of germinated seeds from WT, *mee45-1* or *ant-T* mutants at the indicated hours after seed hydration without aging treatment.

Supplemental Data Set S4. Supplemental Figure S2H data: Number of germinated seeds from WT, *mee45-1* or *ant-T* mutants at the indicated hours after seed hydration with aging treatment.

Supplemental Data Set S5. Supplemental Figure S1H data: Seed mass per 1,000 seeds of the WT, *mee45-2* and *mee45-3*.

Supplemental Data Set S6. Supplemental Figure S1I data: Seed length and width of the WT, *mee45-2* and *mee45-3*.

Supplemental Data Set S7. Supplemental Figure S5I data: Epidermal cell areas in the cotyledons of the WT, *mee45-1*, *mee45-1 MEE45pro:MEE45* and *MEE45pro:MEE45*.

Supplemental Data Set S8. Supplemental Figure S5J data: Cotyledon areas of the WT, *mee45-1*, *mee45-1 MEE45pro:MEE45* and *MEE45pro:MEE45*.

Supplemental Data Set S9. Supplemental Figure S5K data: Epidermal cell number in the cotyledons of the WT, *mee45-1*, *mee45-1 MEE45pro:MEE45* and *MEE45pro:MEE45*.

Supplemental Data Set S10. Supplemental Figure S8F data: Leaf area of *mee45-1* compared to WT (WT set to 100%).

Supplemental Data Set S11. Supplemental Figure S8G data: Silique length and width of *mee45-1* compared to WT (WT set to 100%).

Supplemental Data Set S12. Figure 3I data: Seed mass per 1,000 seeds for the indicated F_1 and F_2 crosses.

Supplemental Data Set S13. Figure 3J data: Seed length and width for the indicated F_1 and F_2 crosses.

Supplemental Data Set S14. Supplemental Figure S9G data: Seed mass per 1,000 seeds for the indicated F_1 crosses.

Supplemental Data Set S15. Supplemental Figure S9H data: Seed length and width for the indicated F_1 crosses.

Supplemental Data Set S16. Supplemental Figure S10G data: Seed mass per 1,000 seeds for the indicated F_1 crosses.

Supplemental Data Set S17. Supplemental Figure S10H data: Seed length and width for the indicated F_1 crosses.

Supplemental Data Set S18. Figure 4K data: Seed mass per 1,000 seeds for the indicated transgenic lines.

Supplemental Data Set S19. Figure 4L data: Seed length and width for the indicated transgenic lines.

Supplemental Data Set S20. Figure 5C data: Number of cells in the outer integument of mature ovules from WT and *mee45-1* plants.

Supplemental Data Set S21. Figure 5D data: Outer integument length of mature ovules from WT and *mee45-1* plants.

Supplemental Data Set S22. Supplemental Figure S13 data: DEGs in m*ee45-1* siliques compared to the WT.

Supplemental Data Set S23. Supplemental Figure S15G data: Seed mass per 1,000 seeds for the indicated genotypes.

Supplemental Data Set S24. Supplemental Figure S15H data: Seed length and width for the indicated genotypes.

Supplemental Data Set S25. Figure 6L data: Seed mass per 1,000 seeds for the indicated genotypes.

Supplemental Data Set S26. Figure 6M data: Seed length and width for the indicated genotypes.

Supplemental Data Set S27. Figure 7L data: Seed mass per 1,000 seeds for the indicated genotypes.

Supplemental Data Set S28. Figure 7M data: Seed length and width for the indicated genotypes.

Supplemental Data Set S29. Figure 8I data: Seed mass per 1,000 seeds for the indicated genotypes.

Supplemental Data Set S30. Figure 8J data: Seed length and width for the indicated genotypes.

Supplemental Data Set S31. Statistical analysis.

Funding

Conflict of interest

The authors declare no competing interest.

REFERENCES

Adamski NM, Anastasiou E, Eriksson S, O'Neill CM, Lenhard M (2009) Local maternal control of seed size by KLUH/CYP78A5-dependent growth signaling. Proc Natl Acad Sci USA **106**: 20115–20120

Chaudhury AM, Koltunow A, Payne T, Luo M, Tucker MR, Dennis ES, Peacock WJ (2001) Control of early seed development. Annu Rev Cell Dev Biol **17**: 677–699

Cheng Y, Dai X, Zhao Y (2006) Auxin biosynthesis by the YUCCA flavin monooxygenases controls the formation of floral organs and vascular tissues in Arabidopsis. Genes Dev **20**: 1790–1799

Cheng ZJ, Wang L, Sun W, Zhang Y, Zhou C, Su YH, Li W, Sun TT, Zhao XY, Li XG, et al. (2013) Pattern of auxin and cytokinin responses for shoot meristem induction results from the regulation of cytokinin biosynthesis by AUXIN RESPONSE FACTOR3. Plant Physiol **161**: 240–251

Clough SJ, Bent AF (1998) Floral dip: a simplified method for Agrobacterium-mediated transformation of *Arabidopsis thaliana*. Plant J **16**: 735–743

Du L, Li N, Chen L, Xu Y, Li Y, Zhang Y, Li C, Li Y (2014) The ubiquitin receptor DA1 regulates seed and organ size by modulating the stability of the ubiquitin-specific protease UBP15/SOD2 in Arabidopsis. Plant Cell **26**: 665–677

Duan Q, Kita D, Li C, Cheung AY, Wu HM (2010) FERONIA receptor-like kinase regulates RHO GTPase signaling of root hair development. Proc Natl Acad Sci USA **107**: 17821–17826

Elliott RC, Betzner AS, Huttner E, Oakes MP, Tucker WQ, Gerentes D, Perez P, Smyth DR (1996) AINTEGUMENTA, an APETALA2-like gene of Arabidopsis with pleiotropic roles in ovule development and floral organ growth. Plant Cell **8**: 155–168

Fan C, Yu S, Wang C, Xing Y (2009) A causal C-A mutation in the second exon of GS3 highly associated with rice grain length and validated as a functional marker. Theor Appl Genet **118**: 465–472

Fang W, Wang Z, Cui R, Li J, Li Y (2012) Maternal control of seed size by EOD3/CYP78A6 in *Arabidopsis thaliana*. Plant J **70**: 929–939

Figueiredo DD, Batista RA, Roszak PJ, Köhler C (2015) Auxin production couples endosperm development to fertilization. Nat Plants **1**: 15184

Figueiredo DD, Batista RA, Roszak PJ, Hennig L, Köhler C (2016) Auxin production in the endosperm drives seed coat development in Arabidopsis. Elife **5**: e20542

Garcia D, Fitz Gerald JN, Berger F (2005) Maternal control of integument cell elongation and zygotic control of endosperm growth

are coordinated to determine seed size in Arabidopsis. Plant Cell **17**: 52–60

Guan Y, Meng X, Khanna R, LaMontagne E, Liu Y, Zhang S (2014) Phosphorylation of a WRKY transcription factor by MAPKs is required for pollen development and function in Arabidopsis. PLoS Genet **10**: e1004384

Haughn G, Chaudhury A (2005) Genetic analysis of seed coat development in Arabidopsis. Trends Plant Sci. **10**: 472–477

He S, Sun Y, Yang Q, Zhang X, Huang Q, Zhao P, Sun M, Liu J, Qian W, Qin G, et al. (2017) A novel imprinted gene NUWA controls mitochondrial function in early seed development in Arabidopsis. PLoS Genet **13**: e1006553

Jofuku KD, Omidyar PK, Gee Z, Okamuro JK (2005) Control of seed mass and seed yield by the floral homeotic gene APETALA2. Proc Natl Acad Sci USA **102**: 3117–3122

Kang X, Li W, Zhou Y, Ni M (2013) A WRKY transcription factor recruits the SYG1-like protein SHB1 to activate gene expression and seed cavity enlargement. PLoS Genet **9**: e1003347

Khush G (2003) Productivity improvements in rice. Nutr Rev **61**: S114–116

Kim D, Pertea G, Trapnell C, Pimentel H, Kelley R, Salzberg SL (2013) TopHat2: accurate alignment of transcriptomes in the presence of insertions, deletions and gene fusions. Genome Biol **14**: R36

Klucher KM, Chow H, Reiser L, Fischer RL (1996) The AINTEGUMENTA gene of Arabidopsis required for ovule and female gametophyte development is related to the floral homeotic gene APETALA2. Plant Cell **8**: 137–153

Lampropoulos A, Sutikovic Z, Wenzl C, Maegele I, Lohmann JU, Forner J (2013) GreenGate--a novel, versatile, and efficient cloning system for plant transgenesis. PLoS One **8**: e83043

Leyser O (2005) The fall and rise of apical dominance. Curr Opin Genet Dev **15**: 468–471

Li H, Johnson P, Stepanova A, Alonso JM, Ecker JR (2004) Convergence of signaling pathways in the control of differential cell growth in Arabidopsis. Dev Cell **7**: 193–204

Li N, Li Y (2015) Maternal control of seed size in plants. J Exp Bot **66**: 1087–1097

Li N, Li Y (2016) Signaling pathways of seed size control in plants. Curr Opin Plant Biol **33**: 23–32

Li N, Xu R, Li Y (2019) Molecular networks of seed size control in plants. Annu Rev Plant Biol **70**: 435–463

Li T, Zhang Y, Wang D, Liu Y, Dirk LMA, Goodman J, Downie AB, Wang J, Wang G, Zhao T (2017) Regulation of seed vigor by manipulation of raffinose family oligosaccharides in maize and *Arabidopsis thaliana*. Mol Plant **10**: 1540–1555

Li Y, Zheng L, Corke F, Smith C, Bevan MW (2008) Control of final seed and organ size by the DA1 gene family in *Arabidopsis thaliana*. Genes Dev **22**: 1331–1336

Liu J, Hua W, Hu Z, Yang H, Zhang L, Li R, Deng L, Sun X, Wang X, Wang H (2015a) Natural variation in ARF18 gene simultaneously affects seed weight and silique length in polyploid rapeseed. Proc Natl Acad Sci USA **112**: E5123–5132

Liu L, Tong H, Xiao Y, Che R, Xu F, Hu B, Liang C, Chu J, Li J, Chu C (2015b) Activation of Big Grain1 significantly improves grain size by regulating auxin transport in rice. Proc Natl Acad Sci USA **112**: 11102–11107

Meister RJ, Kotow LM, Gasser CS (2002) SUPERMAN attenuates positive INNER NO OUTER autoregulation to maintain polar development of Arabidopsis ovule outer integuments. Development **129**: 4281–4289

Meng LS, Wang ZB, Yao SQ, Liu A (2015) The ARF2-ANT-COR15A gene cascade regulates ABA-signaling-mediated resistance of large seeds to drought in Arabidopsis. J Cell Sci **128**: 3922–3932

Mizukami Y, Fischer RL (2000) Plant organ size control: AINTEGUMENTA regulates growth and cell numbers during organogenesis. Proc Natl Acad Sci USA **97**: 942–947

Moles AT, Ackerly DD, Webb CO, Tweddle JC, Dickie JB, Westoby M (2005) A brief history of seed size. Science **307**: 576–580

Nole-Wilson S, Krizek BA (2000) DNA binding properties of the Arabidopsis floral development protein AINTEGUMENTA. Nucleic Acids Res **28**: 4076–4082

Ohto MA, Fischer RL, Goldberg RB, Nakamura K, Harada JJ (2005) Control of seed mass by APETALA2. Proc Natl Acad Sci USA **102**: 3123–3128

Ohto MA, Floyd SK, Fischer RL, Goldberg RB, Harada JJ (2009) Effects of APETALA2 on embryo, endosperm, and seed coat development determine seed size in Arabidopsis. Sex Plant Reprod **22**: 277–289

Pagnussat GC, Yu HJ, Ngo QA, Rajani S, Mayalagu S, Johnson CS, Capron A, Xie LF, Ye D, Sundaresan V (2005) Genetic and molecular identification of genes required for female gametophyte development and function in Arabidopsis. Development **132**: 603–614

Robert HS, Park C, Gutièrrez CL, Wójcikowska B, Pěnčík A, Novák O, Chen J, Grunewald W, Dresselhaus T, Friml J, et al. (2018) Maternal auxin supply contributes to early embryo patterning in Arabidopsis. Nat Plants **4**: 548–553

Schnittger A, De Veylder L (2018) The dual face of cyclin B1. Trends Plant Sci **23**: 475–478

Schruff MC, Spielman M, Tiwari S, Adams S, Fenby N, Scott RJ (2006) The AUXIN RESPONSE FACTOR 2 gene of Arabidopsis links auxin signalling, cell division, and the size of seeds and other organs. Development **133**: 251–261

Shomura A, Izawa T, Ebana K, Ebitani T, Kanegae H, Konishi S, Yano M (2008) Deletion in a gene associated with grain size increased yields during rice domestication. Nat Genet **40**: 1023–1028

Smyth DR, Bowman JL, Meyerowitz EM (1990) Early flower development in Arabidopsis. Plant Cell **2**: 755–767

Song XJ, Huang W, Shi M, Zhu MZ, Lin HX (2007) A QTL for rice grain width and weight encodes a previously unknown RING-type E3 ubiquitin ligase. Nat Genet **39**: 623–630

Su YH, Zhou C, Li YJ, Yu Y, Tang LP, Zhang WJ, Yao WJ, Huang R, Laux T, Zhang XS (2020) Integration of pluripotency pathways regulates stem cell maintenance in the Arabidopsis shoot meristem. Proc Natl Acad Sci USA **117**: 22561–22571

Sun Y, Wang C, Wang N, Jiang X, Mao H, Zhu C, Wen F, Wang X, Lu, Z., Yue, G., et al. (2017) Manipulation of auxin response factor 19 affects seed size in the woody perennial *Jatropha curcas*. Sci Rep **7**: 40844

Vandenbussche F, Van Der Straeten D (2004) Shaping the shoot: a circuitry that integrates multiple signals. Trends Plant Sci **9**: 499–506

Wang B, Chu J, Yu T, Xu Q, Sun X, Yuan J, Xiong G, Wang G, Wang Y, Li J (2015) Tryptophan-independent auxin biosynthesis contributes to early embryogenesis in Arabidopsis. Proc Natl Acad Sci USA **112**: 4821–4826

Wang JG, Feng C, Liu HH, Ge FR, Li S, Li HJ, Zhang Y (2016) HAPLESS13-mediated trafficking of STRUBBELIG is critical for ovule development in Arabidopsis. PLoS Genet. **12**: e1006269

Weigel D (1995) The APETALA2 domain is related to a novel type of DNA binding domain. Plant Cell **7**: 388–389

Weijers D, Geldner N, Offringa R, Jürgens G (2001) Seed development: early paternal gene activity in Arabidopsis. Nature **414**: 709–710

Westermann J, Streubel S, Franck CM, Lentz R, Dolan L, Boisson-Dernier A (2019) An evolutionarily conserved receptor-like kinases signaling module controls cell wall integrity during tip growth. Curr Biol **29**: 3899–3908.e3893

Xia T, Li N, Dumenil J, Li J, Kamenski A, Bevan MW, Gao F, Li Y (2013) The ubiquitin receptor DA1 interacts with the E3 ubiquitin ligase DA2 to regulate seed and organ size in Arabidopsis. Plant Cell **25**: 3347–3359

Yamaguchi N, Wu MF, Winter CM, Berns MC, Nole-Wilson S, Yamaguchi A, Coupland G, Krizek BA, Wagner D (2013) A molecular framework for auxin-mediated initiation of flower primordia. Dev Cell **24**: 271–282

Yao X, Chen J, Zhou J, Yu H, Ge C, Zhang M, Gao X, Dai X, Yang ZN, Zhao Y (2019) An essential role for miRNA167 in maternal control of embryonic and seed development. Plant Physiol **180**: 453–464

Yu F, Li J, Huang Y, Liu L, Li D, Chen L, Luan S (2014) FERONIA receptor kinase controls seed size in *Arabidopsis thaliana*. Mol Plant **7**: 920–922

Zhang Y, Du L, Xu R, Cui R, Hao J, Sun C, Li Y (2015) Transcription factors SOD7/NGAL2 and DPA4/NGAL3 act redundantly to regulate seed size by directly repressing KLU expression in *Arabidopsis thaliana*. Plant Cell **27**: 620–632

Zhang Z, Tucker E, Hermann M, Laux T (2017) A molecular framework for the embryonic initiation of shoot meristem stem cells. Dev Cell **40**: 264–277.e264

Zhou Y, Zhang X, Kang X, Zhao X, Zhang X, Ni M (2009) SHORT HYPOCOTYL UNDER BLUE1 associates with MINISEED3 and HAIKU2 promoters in vivo to regulate Arabidopsis seed development. Plant Cell **21**: 106–117

Zuo J, Li J (2014) Molecular genetic dissection of quantitative trait loci regulating rice grain size. Annu Rev Genet **48**: 99–118